„POLITEHNICA" UNIVERSITY OF BUCHAREST
DOCTORAL SCHOOL OF AEROSPACE ENGINEERING

PHD THESIS SUMMARY

A study on the destructive atmospheric reentry of aerospace vehicles

Author: Ing. Tudorel-Petronel AFILIPOAE

PhD supervisor: Prof. dr. Eng. Teodor-Viorel CHELARU

DOCTORATE COMMITTEE

Chairman	Prof. dr. Eng. Teodor Lucian GRIGORIE	from	POLITEHNICA University of Bucharest
PhD supervisor	Prof. dr. Eng. Teodor-Viorel CHELARU	from	POLITEHNICA University of Bucharest
Reviewer	Prof. dr. Eng. Sterian DANAILA	from	POLITEHNICA University of Bucharest
Reviewer	Prof. dr. Eng. Edward RAKOSI	from	„Gheorghe Asachi" Technical University - Iași
Reviewer	CSII. dr. Eng. Victor PRICOP	from	„Elie Carafoli" National Institute of Aerospace Research

BUCHAREST
2022

Table of contents

1 Introduction 5
1.1 Computational tools for assessing the risk of atmospheric re-entry 5
1.2 Objectives 7
1.3 Thesis content 7
2 Destructive re-entry problem overview 10
3 Geometry generation and inertial properties estimation 12
3.1 Geometry generation 12
3.2 Inertial properties estimation 13
3.3 Inertial properties – Results and validation 13
4 Simulation of six degrees of freedom motion 15
4.1 Reference systems and coordinates transformations 15
4.2 External forces and moments 16
4.3 Equations of motion 17
4.4 Adaptive Runge-Kutta methods 18
4.5 Results and validation 18
5 Simulation of unsteady heat transfer 20
5.1 Numerical solution of the heat equation 20
5.1.1 Spatial discretization using the finite volume method 20
5.1.2 Temporal discretization 21
5.1.3 Initial and boundary conditions 21
5.1.4 Aspects regarding the analytical solution of the heat equation 22
5.2 Results and validation 22
6 Aerodynamics and aerothermodynamics 24
6.1 Aerodynamic properties 24
6.2 Convective heat flux 25
6.3 Validation of the computational models 25
7 Models of thermal destruction of aerospace vehicles re-entering the atmosphere 27
7.1 Ablation model for debris re-entering the atmosphere 27
7.2 Ablation model validation 28
7.3 Simulation of the destructive re-entry of a metalic object 29
7.4 Fragmentation model of complex structures re-entering the atmosphere 30
7.5 Overview of the practical implementation of the computational models 31

7.6 Simulation of the destructive re-entry of a typical rocket stage 31
8 Effect of uncertainties 33
8.1 Introduction 33
8.2 Theoretical aspects regarding the number of iterations and accuracy of a Monte Carlo simulation 33
8.3 Monte Carlo analysis of a destructive atmospheric re-entry. Example case 33
9 Final chapter 35
9.1 Thesis contributions 35
9.2 Conclusions and possibilities for further development 37
9.3 List of publications 39

1 Introduction

Given the growing interest in space exploration, the number of space missions is constantly increasing, bringing with it a significant increase in the number of debris in Earth orbit. At the same time, a large majority of these space missions are designed to include at least one re-entry event of a vehicle or parts of a vehicle (launcher stages, re-entry capsules, etc.). Once re-entered the atmosphere, the debris resulting from space missions is a hazard to the population, fauna, flora and property. For this reason, there is a growing interest in the scientific community to quantify the risk that space debris poses. One measure in this regard is to design computational tools capable of simulating the re-entry of space debris into the atmosphere and thus quantifying the risk associated with a space mission.

This thesis includes a series of studies on the destructive atmospheric re-entry of a vehicle or space debris. Understanding and simulating destructive atmospheric re-entry requires the expertise of several branches of engineering, which is why the thesis includes studies on trajectory analysis, structural analysis, heat transfer, aerodynamics and aerothermodynamics. The aim of these studies is to identify a series of mathematical models that can facilitate the understanding of the phenomena governing atmospheric re-entry, and at the same time to implement and validate these models in a multidisciplinary computational tool capable of simulating a destructive re-entry.

Keywords: *destructive re-entry, space debris, convective heat flux, heat transfer, finite volumes, unstructured grids, trajectory simulation, fragmentation model, ablation model, aerodynamic characteristics, pressure coefficient*

1.1 Computational tools for assessing the risk of atmospheric re-entry

There are currently two main approaches to developing computational environments capable of estimating the risk of re-entry of space debris: *object-based* codes and *vehicle-based* codes.

Object-based computational environments are generally based on several simplifying assumptions compared to vehicle-based ones. Specifically, object-based codes reduce the analysis of the destruction of a given spacecraft to the analysis of the destruction of its component parts. Thus, the components of the analyzed vehicle, often only the critical ones, are modeled as objects with basic geometry such as spheres, cubes, parallelepipeds, cylinders, bars, etc., thus significantly reducing the preprocessing stage prior to a simulation. Each basic object of the vehicle structure is associated with a material that can be either the material of the part modeled by that object, in the case of homogeneous and isotropic objects (metal components), or an equivalent material, in the case of objects containing more than one material and / or are made of composite materials. Object codes are based on the assumption that the structure of the analyzed vehicle will decompose into its component parts (spheres, cubes, etc.) at an altitude that can vary between 75 km and 85 km. From the moment of fragmentation, the resulting objects are subjected to simple thermal analyzes in order to predict the probability of their survival during re-entry and possible impact areas, if they survive. The points of impact of objects that survive re-entry can be extended to areas between 200 and 2000 km in size, depending on the masses of the objects and the properties of the materials from which they are made.

An advantage of object-based codes is that, if the analyzed vehicle breaks down into its component parts, the most unfavorable re-entry scenario is created, one in which the total area exposed to thermal loads during re-entry is maximized. This approach is conservative in the sense that if the analyzed objects survive this worst-case scenario, then they can certainly be considered critical in terms of the risk of impact. Another advantage of object-based codes is the very short computation time, due to the large number of simplifying assumptions. The calculation time for an object code can range from a few seconds to a few minutes ([1]). The disadvantage of object-based codes is that a detailed analysis of the thermal or mechanical processes that take place in the real vehicle during re-entry is not possible, such as rapid heating of parts directly exposed to thermal loads and slower heating of parts that are more protected from these loads.

Some of the most important object-based codes developed by the space community over the years are *Debris Assessment Software* (*DAS*, [2], [3]), *Object Oriented Surveillance Analysis Tool* (*ORSAT*, [4], [5]), *DEBRISK* ([6], [1]), *Debris Risk Assessment and Mitigation Analysis* (*DRAMA*, [1], [7]) and *Spacecraft Aerothermal Model* (SAM, [1], [8]).

Unlike object-based codes, vehicle-based codes model the entire analyzed vehicle as a single entity. Thus, the component parts represent faithful computational models of the real parts that make up the analyzed vehicle. These are materialized in the calculation process by three-dimensional computational grids that form the basis of more complex thermal and aerodynamic analyzes than in the case of object-based codes. Based on the computational grids created, engineering methods are used to estimate convective and radiative heat fluxes and pressure coefficient that will be further used to propagate the thermal state of the vehicle and determine the aerodynamic force acting on it. The propagation of the vehicle trajectory and the resulting debris is achieved by integrating the complete set of equations of motion in 6 degrees of freedom. Structural fragmentation is predicted by monitoring local temperature and mechanical stresses. Thus, the fragmentation takes place by melting, due to exceeding the melting temperature, and by breaking due to exceeding the ultimate mechanical stresses. In most cases, vehicle-based codes are augmented with databases containing material properties that can vary with temperature.

The major advantage of vehicle-based codes is that they offer the possibility of a more complex analysis of the destructive re-entry process, especially in terms of how the fragmentation of the vehicle is modeled based on local mechanical temperatures and stresses, as opposed to object-based codes which impose an a priori established altitude of fragmentation. On the other hand, vehicle-based codes require a much longer computation time than object-based codes, ranging from a few hours to a few days ([1]), depending on the complexity of the vehicle under analysis.

Among the vehicle type codes developed by the space community we can list *Spacecraft Atmospheric reentry and Aerothermal Break-up* (*SCARAB*, [9], [10]), *Spacecraft Aerothermal Model* (*SAM*) and PAMPERO ([11], [12]).

1.2 Objectives

The problem of destructive atmospheric re-entry of an aerospace vehicle is one with a strong multidisciplinary character and its understanding and simulation requires the interconnection of several branches of engineering, both computationally and experimentally. Therefore, the present thesis does not propose an extensive approach to the problem of destructive re-entry but has as *general* objective the identification of a collection of computational models that can make it possible to understand and simulate it. At the same time, the identified mathematical models will be implemented in computational tools and validated with experimental and numerical results, where available. New contributions to the scientific community in the context of destructive re-entry will be made both by supplementing or improving existing mathematical models and by unifying them in a multidisciplinary computing environment. Therefore, among the *specific* objectives of this thesis we can list:

- Implementation and validation of a motion simulator with three and six degrees of freedom in order to propagate the trajectories of the fragments resulting from a destructive re-entry.
- Implementation and validation of a computer program that simulates the heat transfer in solid materials, in order to monitor the thermal state of the fragments resulting from re-entry.
- Implementation and validation of a calculation module for estimating the aerodynamic properties and the convective heat flow for the fragments resulting during re-entry, depending on the flight regime.
- Proposing and implementing models of destruction, burning, breaking, etc. of typical aerospace structures under thermal and / or mechanical loads during re-entry.
- Development and implementation of a data structure for the computational modeling of complex structures specific to aerospace vehicles, compatible with the data structure necessary to evaluate the thermal state, aerodynamic properties, convective heat flow and inertial properties for the resulting fragments.
- Propose a methodology for assessing the influence of modeling uncertainties on the results provided by a suite of computer programs designed to simulate atmospheric destructive re-entry.

1.3 Thesis content

This thesis is divided into 10 chapters depending on the different engineering disciplines involved in addressing the problem of atmospheric destructive re-entry. The contents of each chapter of this thesis are briefly presented below.

Section 1 of this thesis is introductory and presents the current context regarding the issue of space debris. The different approaches of the scientific community to assessing the risk of a space mission to the population, the environment and property are also discussed here. In this context, the main objectives of the thesis will be formulated and the content of each chapter will be briefly presented.

Section 2 provides an overview of the atmospheric destructive re-entry of aerospace vehicles. Here are discussed the phenomena whose understanding are key factors in solving the problem of destructive re-entry and at the same time a preliminary structure of a computational tool dedicated to this problem is identified.

Section 3 presents details on modeling the structure of an aerospace vehicle in a computational tool that simulates atmospheric destructive re-entry. The vehicle will be materialized at the computational level through a collection of computational grids associated with some basic objects that make up the structure. Furthermore, we will present the mathematical model for calculating the inertial properties of the analyzed vehicle and finally we will present a set of results in order to provide a preliminary validation of the mathematical model implementation.

Section 4 presents the theoretical and numerical aspects of simulating the motion with six degrees of freedom of an aerospace vehicle. Specifically, we will discuss aspects such as reference systems and the transformations between them, the state variables chosen for the complete representation of the vehicle state, the mathematical representation of the kinematic and dynamic equations of motion relative to different reference systems and numerical solution methods. We will also exemplify the numerical solution of the equations of motion in the concrete case of the atmospheric re-entry of a capsule, providing at the same time a preliminary validation of the implemented numerical methods.

Section 5 deals with the numerical solution of the unsteady heat equation. Specifically, the focus will be on a cell-centered finite volume method applied to three-dimensional unstructured grids. We will exemplify the numerical solution of the heat equation in the concrete case of an aluminum object, providing also a preliminary validation of the implemented numerical methods.

Section 6 presents the methods adopted to determine the aerodynamic characteristics of the vehicle under analysis as well as the convective heat flux to its surface during atmospheric re-entry. We turn our attention largely to low-fidelity engineering methods because a faithful aerodynamic and aerothermodynamic analysis is not of practical interest in the context of the present problem. Therefore, we will distinguish between three flight regimes, namely the free molecular regime, the rarefied transitional regime and the continuous regime, for which we will adopt different methodologies for estimating the aerodynamic properties and the convective heat flow. At the same time, we will exemplify the process of calculating the aerodynamic properties and convective heat flux in the case of a reentry capsule and we will validate the implemented models using results provided by high fidelity numerical models present in the literature.

Section 7 presents details on the fusion between different mathematical models presented throughout this thesis in order to simulate the destructive re-entry of space vehicles and debris. First, we will propose an ablation model that is appropriate for the destructive re-entry of metal objects that encompasses the motion simulation, heat transfer, aerodynamics and aerothermodynamics models discussed during the previous chapters. The ablation model will be validated using experimental results present in the literature and finally we will exemplify the model in the case of a destructive re-entry of an aluminum object. Secondly, we will propose a model of fragmentation of complex structures which, unlike the simple ablation model mentioned above, is able to monitor the structural integrity of the vehicle but also of the individual objects that make it up. The fragmentation algorithm will be tested on a typical launcher structure. Finally, we will provide an overview of the practical implementation of all computational models that make possible a complex simulation of an atmospheric destructive re-entry.

Section 8 presents a possible approach to quantifying the uncertainty of the results provided by a computational tool that simulates an atmospheric destructive re-entry. We turned our attention to a Monte Carlo-type statistical analysis that involves repetitive simulation of models based on uncertainty ranges associated with the implemented methods and their parameters. We will also discuss the possibility of determining the minimum number of simulations required in order to obtain a desired accuracy of the results. Finally, we will exemplify such a statistical analysis in the case of atmospheric destructive re-entry of a metallic object.

Section 9 presents the final conclusions of this thesis, highlighting its contributions, prospects for further development and the list of scientific papers published during the elaboration of the thesis. The thesis ends with lists of figures, tables and bibliographic references.

2 Destructive re-entry problem overview

The analysis of the destruction of a spacecraft in the atmosphere during re-entry is a multidisciplinary problem that requires the interconnection of several engineering disciplines in order to capture the essential physical aspects associated. Therefore, we can identify several disciplines or modules of analysis that should be considered in the process of developing a computational tool to simulate destructive re-entry:

- *Geometry generation* - A first step in simulating the destructive re-entry of a vehicle is the computational approximation of its structure. We will turn our attention here to an approach in which we will approximate the complex structure of the vehicle by superimposing several objects with simple geometry. For each of these simple objects we will generate a computational grid that will be the basis for further analysis.
- *Grid preprocessing* - This analysis module is responsible for defining the data structure specific to numerical methods that require computational grids such as finite volume or finite element numerical methods for thermal and structural analysis.
- *Inertial properties* - In case of destructive re-entry it is natural to assume that the structure of the analyzed vehicle is altered during re-entry in the presence of thermal and mechanical loads to which it is subjected. For this reason, inertial properties such as mass, center of mass or inertia tensor need to be recalculated as the structure is altered.
- *Aerodynamics* - This module is responsible for assessing the aerodynamic properties of the vehicle, based on the current state of its structure. The aerodynamic properties will be the basis for estimating the forces and moments acting on the vehicle that will be provided to a motion propagator. Other information such as the surface pressure distribution of the vehicle may be potential input data for the structural analysis module.
- *Aerothermodynamics* - The objective of this module is to estimate the heat flux at the surface of the analyzed vehicle. This is further provided as input to a thermal analysis module.
- *Thermal analysis* - Based on the estimated heat flow at the vehicle boundary, this module estimates the evolution of its thermal state. The information determined in this module can be input to a structure fragmentation module and / or a structural analysis module.
- *Structural analysis* - This module is responsible for estimating the stresses that occur in the structure of the vehicle in the presence of thermal and mechanical loads. These will be further provided to a module that monitors the structural integrity of the vehicle.
- *Motion Simulation* - Based on the inertial properties, estimated forces and moments and the previous state of the vehicle, this module calculates its new state. The new state will then be used in a new iteration for estimating the aerodynamic properties and the convective heat flow, the whole process having an iterative character.
- *Fragmentation* - This module monitors the structural integrity of the vehicle based on the information provided by the thermal and structural analysis modules.

Figure 1 shows a generic diagram illustrating the interconnection between different analysis modules. It is important to note that the degree of fidelity of the computational models specific to a module or discipline, or the need to use a certain module of analysis, may depend on the different flight regimes that the vehicle will encounter during re-entry, as we will see in more detail in the following chapters. For example, different aerodynamic models with varying degrees of fidelity may be required depending on the flight regime or various other criteria. On the other hand, the use of a structural analysis module may be impractical, for example, for a fragment detaching from the basic structure of the vehicle. Figure 2 shows a summary of the different types of analyzes that can be used, depending on the different flight regimes.

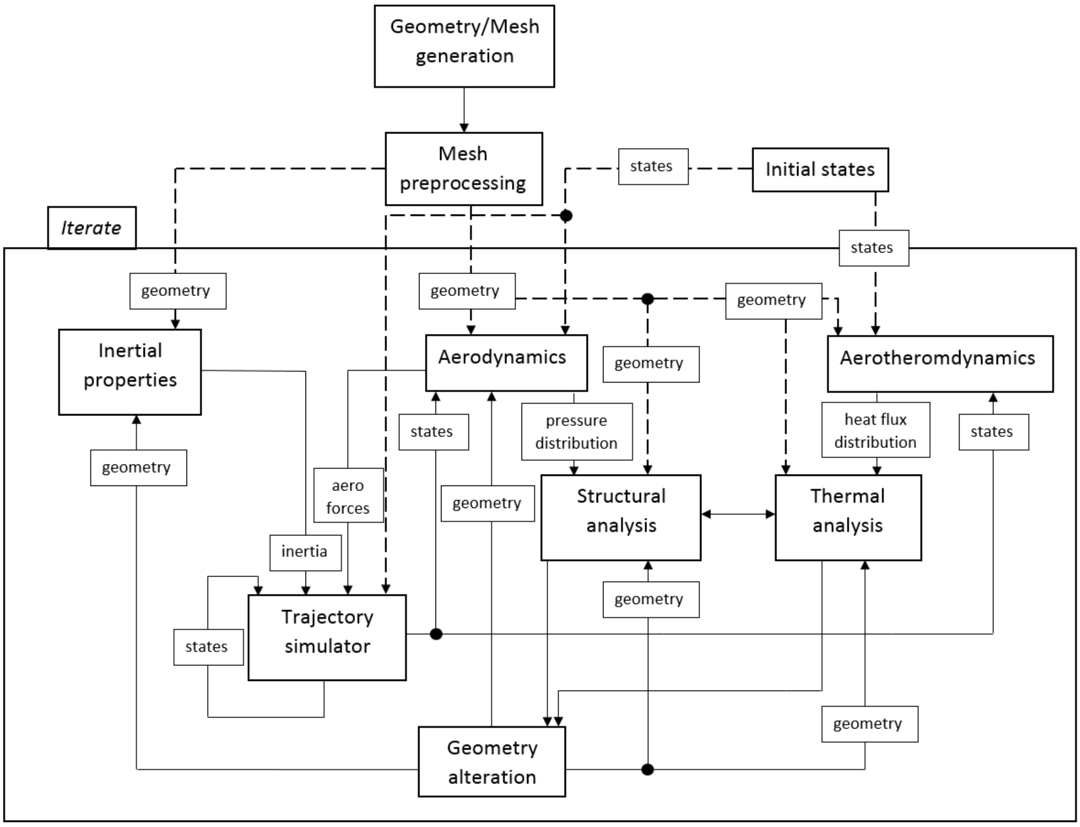

Figure 1 Generic logical scheme for intercommunication between several disciplines

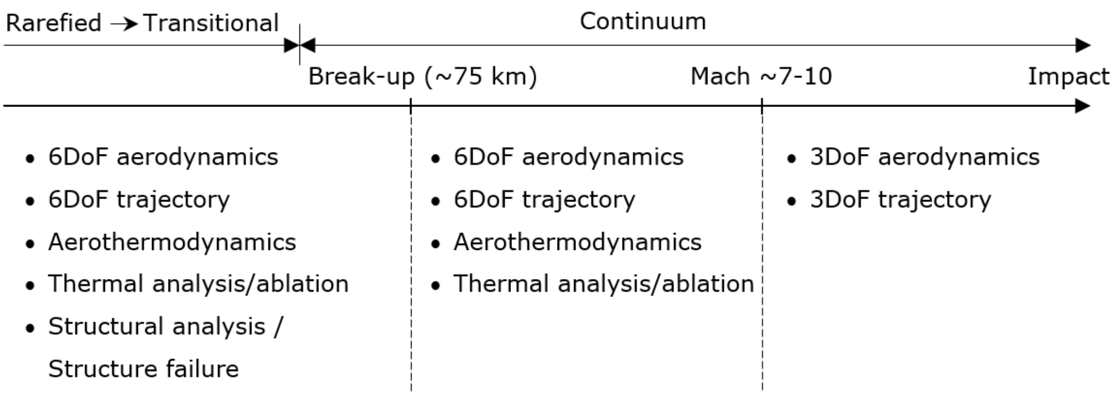

Figure 2 Different analyses to be performed depending on flight regime

3 Geometry generation and inertial properties estimation

3.1 Geometry generation

The vehicle is materialized at the computational level through a collection of computational grids associated with some basic objects that make up the structure. The geometry of these basic objects, hereinafter referred to as *primitives*, is simple (cubes, parallelepipeds, plates, spheres, etc.) and therefore the process of generating computational grids on them is simple as well. Based on input parameters (length, width, diameter, etc.), the coordinates of the nodes (points, in the mathematical sense) that will make up the grid are successively generated in three-dimensional space, similar to the generation of a structured i-j-k type grid. For primitives with more irregular geometry that can be obtained by extrusion (2D to 3D extension), the grid generation module also includes an algorithm that uses the Delaunay two-dimensional triangulation method to generate two-dimensional grids, followed by three-dimensional expansion. The ability to import grids from the CATIA commercial program is also included. Figure 3 shows some examples of primitives that can be generated.

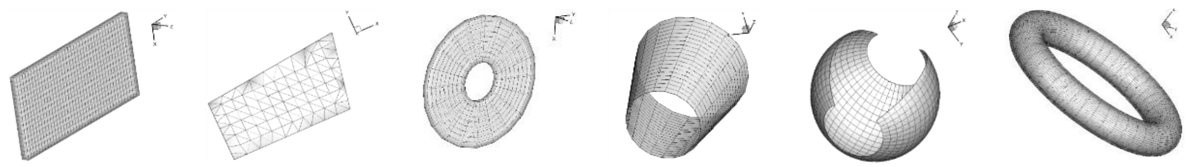

Figure 3 Examples of primitives

Once the computational grids for primitives are generated, the data structure specific to the different methodologies in which the grids are used is generated. This process is associated with the preprocessing module mentioned in Section 2. The information provided by the preprocessing module is divided into three categories: *connectivity*, *geometric properties*, and *boundary information*.

The geometry of each primitive is generated relative to its own reference system that we will note with L. In order to generate the entire structure of the vehicle, they are assembled in a conveniently chosen reference system, noted G. Given the position of the local frame of a primitive i relative to the origin of the global reference system, $\boldsymbol{R}_{L_i}$, and the rotation matrix that determines the relative orientation of the two reference systems L and G, $\boldsymbol{C}_{GL_i}$, the new coordinates of the nodes that define the primitive i in the global reference system of the assembly (see also Figure 4) will be given by:

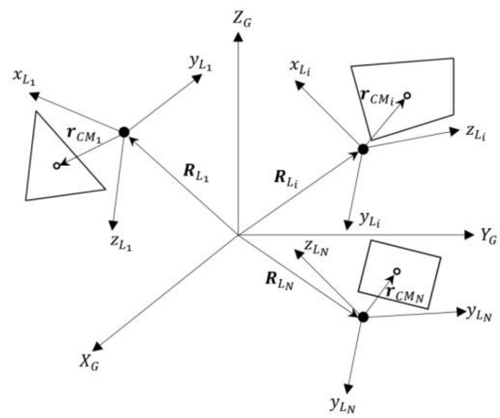

Figure 4 Assembly of primitives

$$\boldsymbol{R}_i = \boldsymbol{R}_{L_i} + \boldsymbol{C}_{GL_i}\boldsymbol{r}_i \,, \tag{3.1}$$

where $\boldsymbol{r}_i$ represents the coordinates of the nodes relative to the local reference system L.

3.2 Inertial properties estimation

As pointed out in the previous chapters, the structure of the vehicle is materialized at the computational level by polyhedral computational grids. Since at the lower level the structure of the vehicle is a reunion of polyhedrons, the calculation of inertial properties is reduced to the calculation of these properties for a polyhedron. In this regard, the methodology proposed in [13] will be used. Assuming a material of constant density, the mass, center of mass and inertial tensor of a polyhedron are defined as:

$$\begin{gathered} m_p = \rho \int_V dV , \\ x_{CM}^p = \frac{\int_V xdV}{\int_V dV}, \quad y_{CM}^p = \frac{\int_V ydV}{\int_V dV}, \quad y_{CM}^p = \frac{\int_V zdV}{\int_V dV}, \\ I_{xx}^p = \rho \int_V (y^2 + z^2) dV, \quad I_{yy}^p = \rho \int_V (x^2 + z^2) dV, \quad I_{zz}^p = \rho \int_V (x^2 + y^2) dV , \\ I_{xy}^p = \rho \int_V xydV, \quad I_{yz}^p = \rho \int_V yzdV, \quad I_{xz}^p = \rho \int_V xzdV , \end{gathered} \tag{3.2}$$

where ρ and V represent the density of the material and the volume bounded by the polyhedron, respectively. The strategy proposed in [13] involves the analytical calculation of volume integrals by transforming them into surface integrals, and considering the hypothesis that the outer surface of the polyhedron consists of triangular elements. Thus, closed analytical formulas result for the inertial properties of the polyhedron. The inertial properties of the vehicle are determined by summing the contributions of all the polyhedrons that make it up. Details are provided in the doctoral thesis and in [13].

3.3 Inertial properties – Results and validation

For the validation of inertial properties calculation models, some examples with simple geometry will be considered. As reference values we will use the inertial properties calculated with the CATIA commercial software. The computational grids were also generated in CATIA and then imported into the implemented models. As an additional measure of validation, an assembly of all considered objects was also generated (see Figure 5), whose inertial properties were calculated both in CATIA and through the implemented models. The results are shown in Table 1 below. Here, the inertial properties of objects are given relative to their center of mass, while those of the assembly are calculated relative to the center of mass of the rectangular parallelepiped (see Figure 5 left). The material considered was steel, with a density of 7860 kg / m3. Very small errors can be observed between the calculated inertial properties and those provided by CATIA. Since the implemented calculation model calculates the exact properties at the level of polyhedral element, the small errors appear exclusively due to the alteration of the geometry following the discretization, higher as the object in question has more curved surfaces. Therefore, as expected, the largest error of 1.73% is recorded in the case of the sphere.

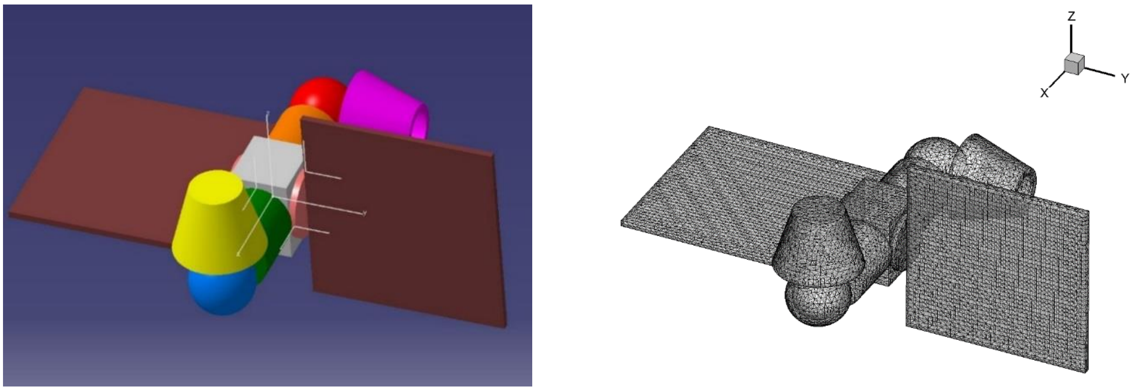

Figure 5 Assembly of selected objects; CATIA model (left) and discretized model (right)

Table 1 Inertial properties of objects and assembly – comparison with results provided by CATIA

		$m\ [kg]$	I_{xx} $[kgm^2]$	I_{yy} $[kgm^2]$	I_{zz} $[kgm^2]$	I_{xy} $[kgm^2]$	I_{xz} $[kgm^2]$	I_{yz} $[kgm^2]$
Rectangular parallelepiped	CATIA	543.283	16.298	17.675	13.111	0	0	0
	Computed	543.2832	16.2985	17.6748	13.1112	-6.9E-17	-4.1E-17	-1.5E-16
	Error [%]	3.68E-05	0.3E-2	0.1E-2	0.18E-2	-	-	-
Rectangular plate	CATIA	452.736	54.389	54.389	108.657	0	0	0
	Computed	452.736	54.3887	54.3887	108.6566	-4.2E-16	-6.7E-15	6.24E-17
	Error [%]	1.30E-12	0.58E-3	0.58E-3	0.33E-3	-	-	-
Sphere	CATIA	263.391	4.214	4.214	4.214	0	0	0
	Computed	260.6606	4.1418	4.1413	4.1421	8.94E-05	-0.31E-3	0.1E-3
	Error [%]	1.04	1.71	1.73	1.71	-	-	-
Thin walled sphere	CATIA	128.535	2.833	2.833	2.833	0	0	0
	Computed	128.001	2.7982	2.7976	2.7981	-4.4E-05	-0.2E-3	-0.26E-3
	Error [%]	0.41	1.23	1.25	1.23	-	-	-
Cylinder	CATIA	395.087	9.219	9.219	7.902	0	0	0
	Computed	393.6804	9.1722	9.1715	7.8456	0.32E-3	2.27E-05	0.17E-3
	Error [%]	0.36	0.51	0.52	0.71	-	-	-
Thin walled cylinder	CATIA	142.231	4.229	4.229	4.665	0	0	0
	Computed	142.256	4.2208	4.2203	4.6475	0.13E-2	0.2E-3	-0.33E-3
	Error [%]	0.18e-1	0.19	0.21	0.37	-	-	-
Conical frustum	CATIA	489.907	12.693	12.693	13.303	0	0	0
	Computed	488.5858	12.6413	12.6409	13.2368	-0.11E-3	8.6E-06	5.58E-05
	Error [%]	0.27	0.41	0.41	0.49	-	-	-
Thin walled conical frustum	CATIA	164.267	5.712	5.712	7.176	0	0	0
	Computed	164.2522	5.7013	5.7013	7.1519	5.5E-05	-7E-05	0.11E-3
	Error [%]	0.9e-2	0.19	0.19	0.34	-	-	-
Disk	CATIA	39.509	0.4	0.4	0.79	0	0	0
	Computed	39.3699	0.3976	0.3975	0.7846	-1.2E-05	-5.7E-06	-8.1E-07
	Error [%]	0.35	0.60	0.62	0.68	-	-	-
Assembly	CATIA	3111.191	935.285	1004.436	1606.803	-49.926	159.554	-1.397e-4
	Computed	3104.931	933.5309	1000.364	1604.231	-49.9305	158.0749	0.36E-3
	Error [%]	0.20	0.19	0.41	0.16	0.89E-2	0.93	-

4 Simulation of six degrees of freedom motion

This chapter aims to present the theoretical and numerical aspects of simulating the atmospheric flight in six degrees of freedom of an aerospace vehicle. More specifically, aspects such as reference systems and the transformations between them, the state variables chosen for the complete representation of the vehicle state, the mathematical representation of the kinematic and dynamic equations of motion relative to different reference systems and numerical solution methods were discussed. The numerical solution of the equations of motion was exemplified in the case of the atmospheric re-entry of a capsule, having at the same time the objective of providing a preliminary validation of the implemented methods.

4.1 Reference systems and coordinates transformations

The main reference systems used in this thesis to express the state variables of the vehicle, the forces and moments acting on it and the differential equations that govern the motion, are:

- *Inertial geocentric frame* ($Ox_I y_I z_I$, notation I, Figure 6)
- *Non-inertial geocentric frame* ($Ox_R y_R z_R$, notation R, Figure 6)
- *Local vertical frame* ($Ox_V y_V z_V$, notation V, Figure 6)
- *Trajectory frame* ($Ox_{TG} y_{TG} z_{TG}$, notation TG, Figure 7)
- *Body-fixed frame* ($Ox_B y_B z_B$, notation B, rigidly attached to the vehicle, Figure 8)
- *Aerodynamic frame* ($Ox_{AG} y_{AG} z_{AG}$, notation AG, Figure 8)

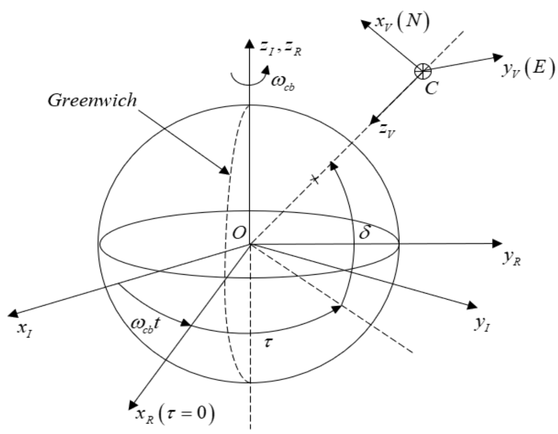

Figure 6 $Ox_I y_I z_I$, $Ox_R y_R z_R$ and $Ox_V y_V z_V$ reference frames

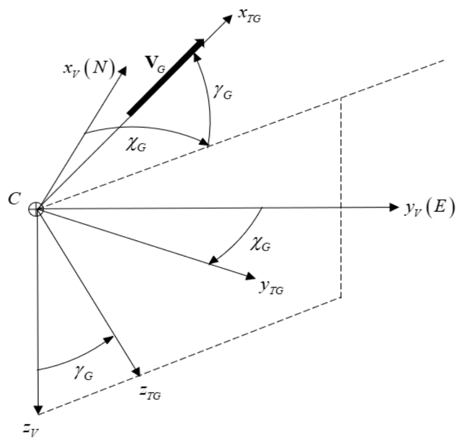

Figure 7 Trajectory reference frame $Ox_{TG} y_{TG} z_{TG}$

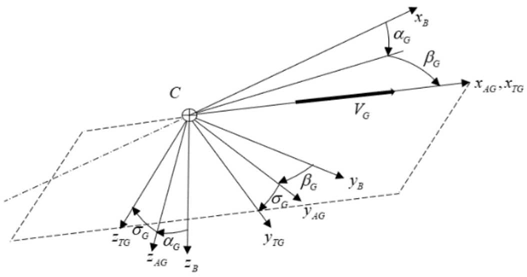

Figure 8 Aerodynamic reference frame $Ox_{AG} y_{AG} z_{AG}$

To fully describe the state of the vehicle in six degrees of freedom, state variables are required to express the position of the center of mass, the velocity of the center of mass, the vehicle attitude and angular velocity. Therefore, three approaches were used for the position and velocity of the center of mass:

- *Inertial cartesian position and velocity (abbreviation PIcVIc)* - $\boldsymbol{r}_{cm,I}$ (x_I ,y_I and z_I) and $\boldsymbol{V}_{i,I}$ ($\dot{x}_I$,$\dot{y}_I$ și $\dot{z}_I$), see Figure 6.
- *Relative position and velocity in spherical coordinates (abbreviation PRpVRp)* – geocentric latitude δ, longitude τ and position vector magnitude r, and flight path angle γ_G, velocity vector azimuth χ_G and relative velocity magnitude V_G, respectively (see Figure 6 and Figure 7).
- *Relative position in spherical coordinates and relative velocity in cartesian coordinates (abbreviation PRpPRc)* - δ, τ and r, and $v_{x,V} = v_\delta$, $v_{y,V} = v_\tau$ and $v_{z,V} = -v_r$, respectively (see Figure 6).

For expressing the vehicle attitude, three approaches were used:

- *Aerodynamic angles (abbreviation Ua)* – angle of attack α_G, sideslip angle β_G and bank angle σ_G (Figure 8).
- *ZYX Euler angles (abbreviation UE)* – roll angle ϕ_V , pitch angle θ_V and yaw angle ψ_V relating the V and B frames.
- *Quaternion (abbreviation Q)* - $\tilde{\boldsymbol{q}} = (q, \boldsymbol{q})$.

The angular velocity of the vehicle is expressed in the frame B, $\omega_{x,B} = p$, $\omega_{y,B} = q$, $\omega_{z,B} = r$.

This chapter also presents the coordinate transformations that make it possible to express the vector quantities of interest in different reference systems. Details are provided in the doctoral thesis.

4.2 External forces and moments

During atmospheric flight, a rigid vehicle of variable mass is subjected to both external forces and moments as well as apparent accelerations. Apparent accelerations, represented by Coriolis acceleration and centrifugal acceleration, are due to the expression of equations with respect to a non-inertial reference system. In the case of the destructive re-entry problem, the external forces and moments are of aerodynamic and gravitational nature.

The *force* and the *aerodynamic moment* are determined based on the aerodynamic properties of the analyzed vehicle (aerodynamic coefficients) and the local atmospheric density. The aerodynamic force can be expressed in the aerodynamic frame or in the body-fixed frame, depending on the available aerodynamic coefficients. For this reason, both possibilities of expressing it were implemented in the calculation program, more details being presented in the thesis. The local atmospheric density is determined using the NRLMSISE00 atmospheric model available in MATLAB. To determine the *gravitational force*, the calculation program implements an advanced model that also considers the spheroidal shape of the Earth. The components of the gravitational force are expressed in both frame R and frame V.

4.3 Equations of motion

This chapter presents the equations that govern the motion of a rigid vehicle with variable mass in atmospheric flight. They are divided into dynamic and kinematic equations which can further be classified to be of translation or rotation. Translation equations can be written relative to an inertial or non-inertial reference system, in Cartesian or spherical coordinates. The kinematic equations of rotation can be expressed using several sets of state variables of which only the aerodynamic angles, the Euler angles and the quaternion are presented. Dynamic equations of rotation are represented by the so-called Euler equations that govern the rotation of a rigid body relative to an inertial reference system.

In order to simulate the motion of the analyzed vehicle in six degrees of freedom, three complete sets of equations of motion were implemented, depending on chosen state variables and reference systems (Table 2). In addition to the fact that each of these sets of equations has certain advantages and disadvantages, highlighted in the thesis, the use of the three sets of equations was also an additional opportunity to validate the correctness of the implementation.

Table 2 State variables chosen for 6DoF motion simulation

	State variables		
	Set 1	Set 2	Set 3
Position of the center of mass	r, τ, δ	r, τ, δ	$\boldsymbol{r}_{cm,I}$
Velocity of the center of mass	V_G, χ_G, γ_G	v_τ, v_δ, v_r	$\boldsymbol{V}_{i,I}$
Attitude	$\alpha_G, \beta_G, \sigma_G$	ϕ_V, θ_V, ψ_V	$\tilde{\boldsymbol{q}}$
Angular velocity	p, q, r	p, q, r	p, q, r

In the following, we will present only the third set (Table 2) of equations of motion while the reader can find details on the other sets of equations in the complete thesis. Therefore, the motion with six degrees of freedom in the context of atmospheric re-entry is governed by the following 13 differential equations:

$$\frac{d\boldsymbol{V}_{i,I}}{dt} = \begin{Bmatrix} \dot{v}_x \\ \dot{v}_y \\ \dot{v}_z \end{Bmatrix}_I = \begin{Bmatrix} \ddot{x} \\ \ddot{y} \\ \ddot{z} \end{Bmatrix}_I = \frac{1}{m}\left(\boldsymbol{F}_{A,I} + \boldsymbol{F}_{G,I}\right), \tag{4.1}$$

$$\frac{d\boldsymbol{r}_{cm,I}}{dt} = \boldsymbol{V}_{i,I} = \begin{Bmatrix} v_x \\ v_y \\ v_z \end{Bmatrix}_I = \begin{Bmatrix} \dot{x} \\ \dot{y} \\ \dot{z} \end{Bmatrix}_I, \tag{4.2}$$

$$\dot{\boldsymbol{\omega}}_B = \boldsymbol{I}^{-1}\left(\boldsymbol{M}_{A,B} - \boldsymbol{\omega}_B \times \boldsymbol{I}\boldsymbol{\omega}_B\right), \tag{4.3}$$

$$\dot{\tilde{\boldsymbol{q}}}_{I,B} = \begin{Bmatrix} \dot{q}_1 \\ \dot{q}_2 \\ \dot{q}_3 \\ \dot{q}_4 \end{Bmatrix} = \frac{1}{2}\begin{bmatrix} -q_4 & -q_3 & q_2 \\ q_3 & -q_4 & -q_1 \\ -q_2 & q_1 & -q_4 \\ q_1 & q_2 & q_3 \end{bmatrix}\begin{Bmatrix} p \\ q \\ r \end{Bmatrix}, \tag{4.4}$$

where $\boldsymbol{F}_{A,I}$, $\boldsymbol{F}_{G,I}$ and $\boldsymbol{M}_{A,B}$ represents the aerodynamic force, the gravitational force and the aerodynamic moment, respectively.

4.4 Adaptive Runge-Kutta methods

Writing the kinematic and dynamic equations of motion of a vehicle in atmospheric flight leads to a system of ordinary first-order nonlinear equations:

$$\dot{\boldsymbol{x}}(t) = \boldsymbol{f}\big(t, \boldsymbol{x}(t)\big)\,, \tag{4.5}$$

with the initial condition:

$$\boldsymbol{x}(t_0) = \boldsymbol{x}_0\,. \tag{4.6}$$

The solution of the system of differential equations was performed numerically, using an adaptive Runge-Kutta method (known as *Runge-Kutta* $p(\hat{p})$):

$$\begin{aligned}
&\boldsymbol{k}_1 = \boldsymbol{f}(t_0, \boldsymbol{x}_0),\\
&\boldsymbol{k}_2 = \boldsymbol{f}(t_0 + c_2 h, \boldsymbol{x}_0 + h a_{21}\boldsymbol{k}_1),\\
&\boldsymbol{k}_2 = \boldsymbol{f}\big(t_0 + c_3 h, \boldsymbol{x}_0 + h(a_{31}\boldsymbol{k}_1 + a_{32}\boldsymbol{k}_2)\big),\\
&\cdots,\\
&\boldsymbol{k}_s = \boldsymbol{f}\Big(t_0 + c_s h, \boldsymbol{x}_0 + h\big(a_{s1}\boldsymbol{k}_1 + \cdots + a_{s,s-1}\boldsymbol{k}_{s-1}\big)\Big),\\
&\boldsymbol{x}_1 = \boldsymbol{x}_0 + h(b_1\boldsymbol{k}_1 + \cdots + b_s\boldsymbol{k}_s),\\
&\widehat{\boldsymbol{x}}_1 = \widehat{\boldsymbol{x}}_0 + h\big(\hat{b}_1\boldsymbol{k}_1 + \cdots + \hat{b}_s\boldsymbol{k}_s\big),
\end{aligned} \tag{4.7}$$

where a_{ij}, b_i and c_i are real constant coefficients and s represents the number of steps of the Runge-Kutta method. The coefficients a_{ij}, b_i and c_i define the so-called Butcher table. The use of such a Runge-Kutta method has the advantage that it provides two approximations of the solution, $\boldsymbol{x}_1$ and $\widehat{\boldsymbol{x}}_1$, which can be used to estimate the time step required to achieve the desired accuracy.

4.5 Results and validation

In this chapter, the six-degree motion of an atmospheric re-entry capsule was analyzed. In order to validate the numerical implementation, the results provided by the three sets of equations mentioned above were compared with the ASTOS 8.0 [14] commercial program, dedicated to simulating trajectories of aerospace vehicles.

The vehicle whose motion was analyzed is the MUSES-C re-entry capsule (Figure 9, [15]). The inertial data of the capsule can be found in Table 1. The trajectory was simulated starting with an initial altitude of 98 km and an initial velocity of 8060 m / s. The initial attitude of the vehicle was defined by a value of 5 degrees for the angle of attack and a value of 8 degrees for the side slip angle. For more details on some aspects of the simulation such as aerodynamic data, initial conditions, parameters of the planet model, atmosphere and gravity, parameters of the numerical solution method, etc., the reader can go through the complete thesis.

For the presentation of the results regarding the translational motion, the altitude H, the longitude τ and the geocentric latitude δ, for the position of the center of mass, and the relative velocity magnitude V_G were plotted. Thus, in Figure 10 and Figure 11 a very good agreement can be seen between the results provided by the three implemented sets of equations and those provided by the ASTOS commercial software. A very good agreement can also be seen for the rotational motion in Figure 12 and Figure 13, where the angle of attack of the capsule was plotted.

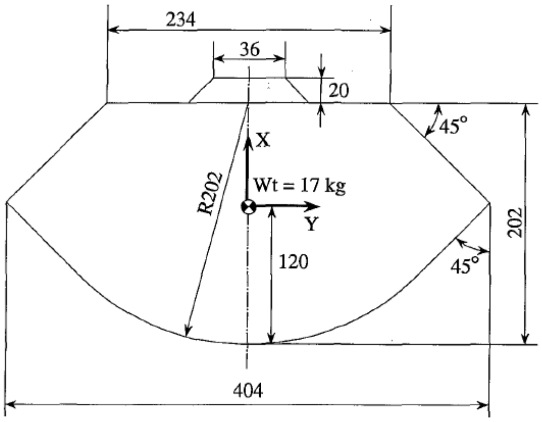

Figure 9 MUSES-C reentry capsule

Table 3 Inertial data of MUSES-C capsule

Mass, m	17.0 kg
Inertia moment, I_{xx}	0.289 kgm^2
Inertia moment, I_{yy}	0.147 kgm^2
Inertia moment, I_{zz}	0.136 kgm^2
Product of inertia, I_{xy}	0.0 kgm^2
Product of inertia, I_{yz}	0.0 kgm^2
Product of inertia, I_{xz}	0.0 kgm^2

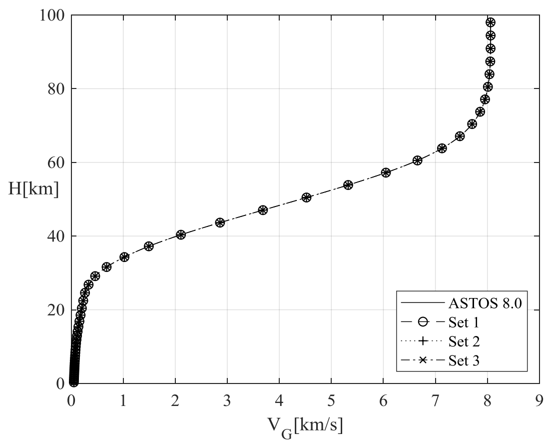

Figure 10 Altitude and relative velocity of MUSES-C capsule

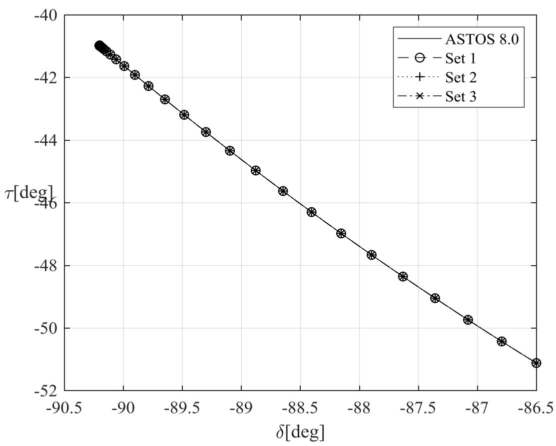

Figure 11 Longitude and geocentric latitude of MUSES-C capsule

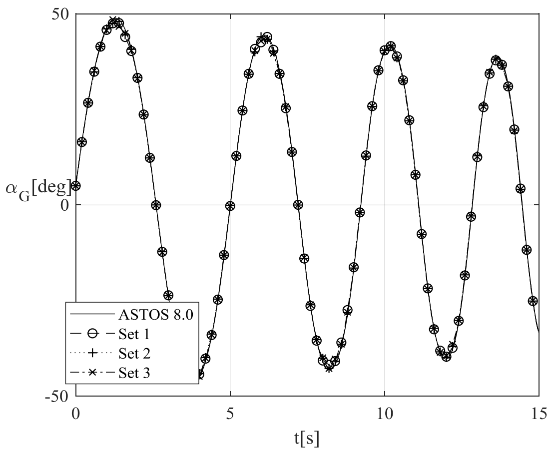

Figure 12 Angle of attack of MUSES-C capsule in the first 15 s of flight

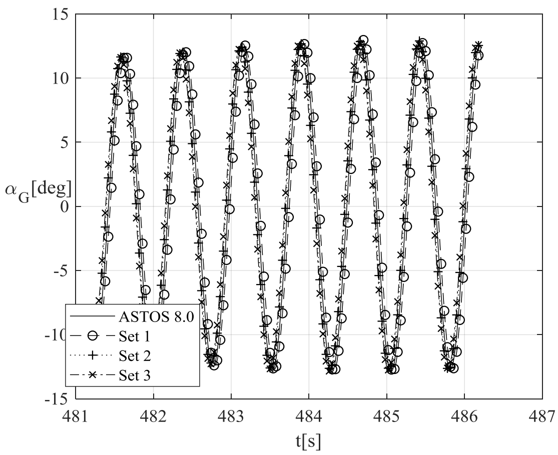

Figure 13 Angle of attack of MUSES-C capsule in the last 5 s of flight

5 Simulation of unsteady heat transfer

One of the specific aspects of atmospheric destructive re-entry is the heat transfer problem. Given the fact that the destruction process of a space debris in the atmosphere is largely thermal in nature, it is necessary to monitor the object's thermal state. This is possible by using the unsteady heat equation:

$$\frac{\partial T}{\partial t} - \alpha \Delta T = \frac{Q}{c\rho}, \tag{5.1}$$

where T represents the absolute temperature, c, ρ and α represent the specific heat, density and thermal diffusivity of the material while Q represents the heat generated inside the material.

This chapter discusses the numerical solution of the unsteady heat equation. Specifically, we will turn our attention to a cell-centered finite volume method applied to three-dimensional unstructured grids. Furthermore, we will exemplify the numerical solution of the heat equation in the case of an aluminum object, providing at the same time a preliminary validation of the implemented numerical methods.

5.1 Numerical solution of the heat equation

5.1.1 Spatial discretization using the finite volume method

The first step in the numerical integration of the heat equation is represented by the so-called discretization of the computational domain. This involves dividing the entire domain bounded by the analyzed object into a finite number of subdomains, called *finite volumes*, *cells*, or *elements* (not to be confused with the finite element method).

A spatial discretization with the finite volume method for the heat equation on an element of the computational grid is written (where the term Q due to internal heat sources was neglected):

$$c\rho V_e \frac{d\bar{T}}{dt} = -R(\bar{T}), \qquad R(\bar{T}) = -\sum_{i=1}^{NF} k \boldsymbol{n}_i \boldsymbol{\nabla} T S_i, \tag{5.2}$$

where k, $\bar{T}$, V_e, $\boldsymbol{n}_i$ and S_i represents the thermal conductivity, the average temperature per element, the volume of the element, the unit normal vectors and the areas of the interfaces that bound the element, respectively. The term R is called heat flux (or explicit operator) and represents the sum of all heat fluxes associated with the interfaces of the element (a total number of NF interfaces).

The temperature gradient for a grid cell required to calculate the heat flux ($\boldsymbol{\nabla} T$) is calculated using the least squares method, taking into account the temperatures in the neighboring cells. Thus, the temperature gradient on a cell i will be a weighted sum such as the following:

$$\boldsymbol{\nabla} T_i = \sum_{j=1}^{N} \boldsymbol{w}_{ij} \left(\bar{T}_j - \bar{T}_i\right), \tag{5.3}$$

where $\bar{T}_j$ represents the temperature in a neighboring cell j. The temperature gradient at the interfaces that bound a cell is calculated by averaging the gradients associated with the cells adjacent to the interfaces. More details on the spatial discretization of the heat equation are provided in the doctoral thesis.

5.1.2 Temporal discretization

For the temporal discretization of the heat equation, an implicit numerical method specially designed for unsteady problems has been used. The method is intensively used in numerical simulation of fluid flows (CFD) and it is called *the dual time method* (Jameson, [16]). The dual time method is based on a second-order time discretization of equation (5.2), from which we obtain:

$$c\rho V_e \frac{3\bar{T}^{n+1} - 4\bar{T}^{n} + \bar{T}^{n-1}}{2\Delta t} = -R^{n+1} \,. \tag{5.4}$$

The solution of the system of differential equations is performed by defining a steady state problem that must be solved at each physical time step. The auxiliary steady state problem is defined similarly to the original problem, namely:

$$c\rho V_e \frac{\partial \bar{T}^*}{\partial t^*} = -R^*(\bar{T}^*) \,, \tag{5.5}$$

where:

$$\begin{gathered} R^*(\bar{T}^*) = R(\bar{T}^*) + c\rho V_e \frac{3}{2\Delta t}\bar{T}^* - Q^* \,, \\ Q^* = \ c\rho V_e \left(\frac{2}{\Delta t}\bar{T}^n - \frac{1}{2\Delta t}\bar{T}^{n-1}\right) \end{gathered} \tag{5.6}$$

Note that the modified numerical flux R^* is defined so that when it is zero, equation (5.4) is fulfilled. For this reason, the solution of the steady state problem is achieved by propagating equation (5.5) in the fictitious time t^*, until the time derivative is canceled and implicitly $R^* = 0$.

The temporal discretization of the stationary problem is performed by means of an implicit numerical scheme:

$$c\rho V_e \frac{\Delta T^\tau}{\Delta t^*} = -{R^*}^{\tau+1} \,, \tag{5.7}$$

where $\Delta T^\tau = {\bar{T}^*}^{\tau+1} - {\bar{T}^*}^{\tau}$ and Δt^* represents the fictitious time step. Discretization (5.7) leads to a system of linear algebraic equations whose matrix (or implicit operator) is sparse. The system of equations is solved using a Gauss-Seidel iterative numerical method.

5.1.3 Initial and boundary conditions

A unique solution of the heat equation can only be determined if the initial and boundary conditions are specified. Imposing the initial condition is often trivial as it only requires the initialization of the vector of unknowns $\bar{T}$. If the initial condition is analytical, it will be calculated in the coordinates of the centers of the grid cells and will be assigned to the corresponding positions in the unknown vector. On the other hand, the boundary conditions must be discretized according to the numerical method chosen for the spatial discretization of the differential equation. This chapter presents the methodology for introducing the influence of the computational domain boundaries on the explicit operator (*explicit boundary conditions*) and on the implicit operator (*implicit boundary conditions*). Details on the methodology for each type of boundary considered (imposed temperature, imposed heat flux, thermal insulation) are presented in the complete thesis.

5.1.4 Aspects regarding the analytical solution of the heat equation

To validate the implemented numerical method, the numerical results were compared with the analytical solution of the heat equation. Thus, the unsteady heat transfer problem in a rectangular parallelepiped having an initial temperature distribution given by a function $f(x,y,z)$ and whose boundaries are maintained at temperature 0, has been solved both analytically and numerically. Considering constant thermal diffusivity, the problem is formulated in this case as follows:

$$\begin{gathered}\frac{\partial T}{\partial t} - \alpha \Delta T = 0, \qquad x,y,z \in D = (0,a) \times (0,b) \times (0,c), \qquad t > 0, \\ CI: \quad T(x,y,z,0) = f(x,y,z), \qquad x,y,z \in D, \\ CL: \quad T(x,y,z,t) = 0, \qquad x,y,z \in \partial D, \qquad t > 0\,. \end{gathered} \tag{5.8}$$

In the case when the initial temperature distribution is given by the function:

$$f(x,y,z) = T_{max} sin\left(\frac{\pi x}{a}\right) sin\left(\frac{\pi y}{b}\right) sin\left(\frac{\pi z}{c}\right), \tag{5.9}$$

the solution of the problem (5.8) will be simply:

$$T^*(x,y,z,t) = f(x,y,z)e^{-\lambda t}, \tag{5.10}$$

where:

$$\lambda = \alpha \pi^2 \left(\frac{1}{a^2} + \frac{1}{b^2} + \frac{1}{c^2}\right). \tag{5.11}$$

5.2 Results and validation

This chapter exemplifies the numerical solution of unsteady conductive heat transfer in the particular case of an aluminum cube of side $l = 0.2\ m$ whose faces are maintained at a constant temperature of 0 K. Starting from an initial temperature distribution given by function (5.9), with $T_{max} = 273.15\ K$ (see Figure 15), the time evolution of the temperature over 20 seconds was analyzed. For this purpose, six computational grids consisting of hexahedral elements were generated, with resolutions ranging from 1000 to 64000 cells (Figure 14).

The evolution over time of the aluminum cube temperature estimated using the implemented numerical methods is given in Figure 16. Figure 17 shows the temperature error in the center of the aluminum cube at $t = 20\ s$, calculated relative to the analytical solution of the heat equation and as a function of the grid resolution and the desired temporal accuracy (CFL number). There can be seen a good ability of the implemented numerical methods to estimate the solution of the unsteady heat equation.

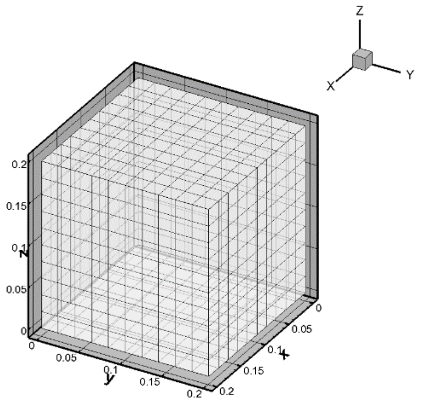

Figure 14 Generic computational grid

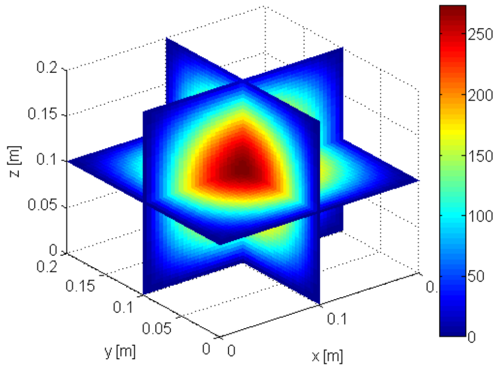

Figure 15 Temperature distribution at $t = 0\ s$

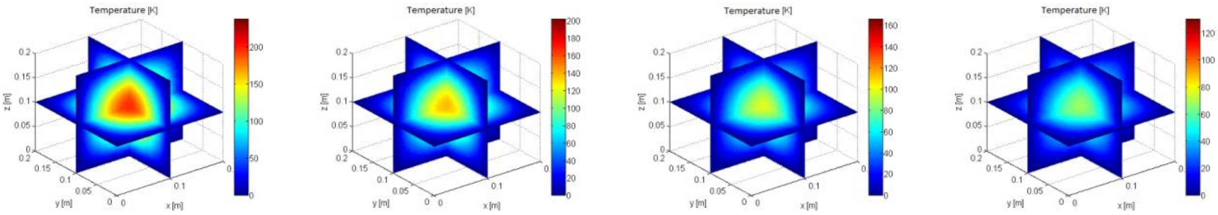

$t = 5\ s$ $t = 10\ s$ $t = 15\ s$ $t = 20\ s$

Figure 16 Temperature evolution of the aluminum cube

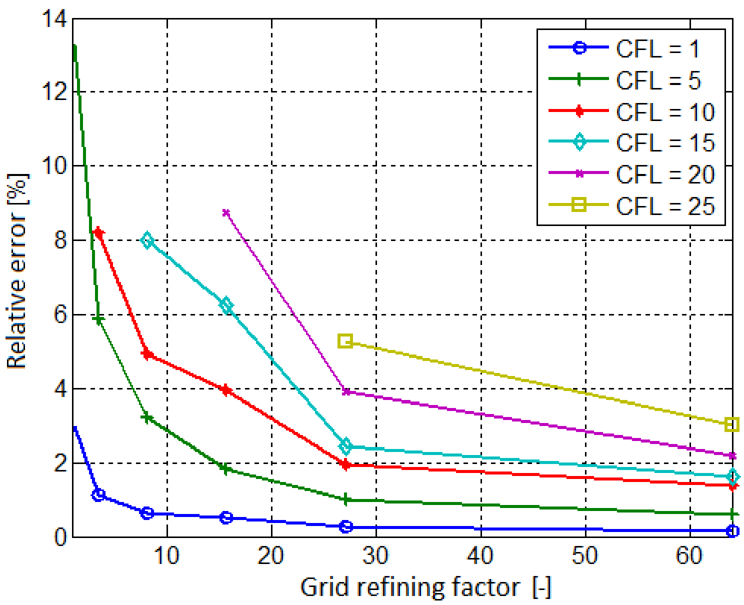

Figure 17 The relative error of the solution at the point $P = (l/2, l/2, l/2)$ and time $t = 20\ s$, as a function of the CFL number

6 Aerodynamics and aerothermodynamics

This chapter aims to present the methods adopted to determine the aerodynamic characteristics of the vehicle under analysis as well as the convective heat flux on its surface during atmospheric re-entry. Attention is largely focused on low-fidelity engineering methods as a faithful aerodynamic and aerothermodynamic analysis is not of practical interest in the context of the present problem. Therefore, a distinction will be made between three flight regimes, namely the free molecular regime, the rarefied transitional regime and the continuous regime, for which different methodologies for estimating aerodynamic properties and convective heat flux will be adopted.

6.1 Aerodynamic properties

For the calculation of the aerodynamic properties of the vehicle we will largely use the so-called *local inclination methods* or *panel methods*. The basic idea of these methods is to discretize the outer surface of the vehicle into a finite number of flat panels, followed by the calculation of the local pressure and friction coefficients on each panel. The latter are then integrated on the entire outer surface of the analyzed vehicle, yielding the aerodynamic force and moment coefficients of the vehicle. Assuming that we have a discretized structure in N panels, the force and moment coefficients will be given by:

$$
\begin{gathered}
\begin{Bmatrix} C_x \\ C_y \\ C_z \end{Bmatrix} = \frac{1}{S_{ref}} \int_S \left(C_p \boldsymbol{n} + C_f \boldsymbol{t} \right) dS \cong \frac{1}{S_{ref}} \sum_{i=1}^{N} \left(C_p \begin{Bmatrix} n_x \\ n_y \\ n_z \end{Bmatrix} + C_f \begin{Bmatrix} t_x \\ t_y \\ t_z \end{Bmatrix} \right)_i S_i \,, \\
\begin{Bmatrix} C_l \\ C_m \\ C_n \end{Bmatrix} = \frac{1}{S_{ref} l_{ref}} \int_S \left[C_p (\boldsymbol{r} \times \boldsymbol{n}) + C_f (\boldsymbol{r} \times \boldsymbol{t}) \right] dS \\
\cong \frac{1}{S_{ref} l_{ref}} \sum_{i=1}^{N} \left[C_p \begin{Bmatrix} (\boldsymbol{r} \times \boldsymbol{n})_x \\ (\boldsymbol{r} \times \boldsymbol{n})_y \\ (\boldsymbol{r} \times \boldsymbol{n})_z \end{Bmatrix} + C_f \begin{Bmatrix} (\boldsymbol{r} \times \boldsymbol{t})_x \\ (\boldsymbol{r} \times \boldsymbol{t})_y \\ (\boldsymbol{r} \times \boldsymbol{t})_z \end{Bmatrix} \right]_i S_i \,,
\end{gathered}
\tag{6.1}
$$

where $\boldsymbol{n}$, $\boldsymbol{t}$, S_i are the inward-facing unit normal, the unit tangent vector, and the area of panel i. The vector $\boldsymbol{r}$ is the position vector of the center of the panel i relative to the center of mass of the vehicle.

Local pressure and friction coefficients are calculated by different methods, depending on the flight regime. Thus, in the case of the free molecular regime, they are calculated based on the molecule-surface interaction theory developed by Schaaf and Talbot [17]. For the rarefied transitional regime, the local pressure and friction coefficients were calculated using bridging functions that correlate the pressure and friction coefficients between the free molecular and continuous regime [18]. In the case of the continuous hypersonic regime, the pressure and friction coefficients were calculated using the modified Newton method ([18], [19]). For low speed regimes (supersonic, transonic, subsonic) only an average drag coefficient is calculated in the form of a profile as a function of Mach number. The profile is built based on anchor points associated with the drag coefficient of some objects with simple geometry and the drag coefficient calculated with the Newton method at the boundary of the hypersonic regime. The method is based on Mccleskey's approach from [20]. Details on the method are presented in the complete thesis.

Since in the hypersonic regime, the pressure and friction coefficients are calculated only on the panels exposed to the air flow, this thesis also proposes an algorithm capable of determining the shaded areas of a vehicle with concave geometry. The algorithm is an improvement on that proposed by Mostaza-Prieto in [21], in that it minimizes the number of panel-to-panel checks and at the same time benefits from the parallelization capabilities available in MATLAB. The algorithm was tested and validated on a toroidal structure (Figure 18, Figure 19).

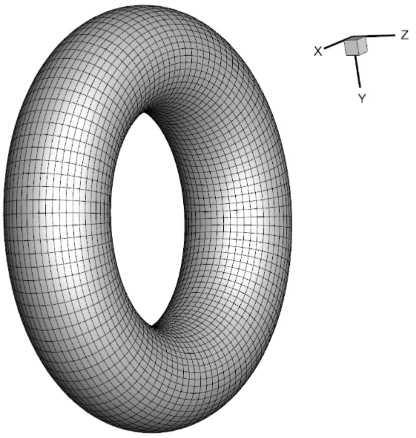

Figure 18 Computational grid on the toroidal object

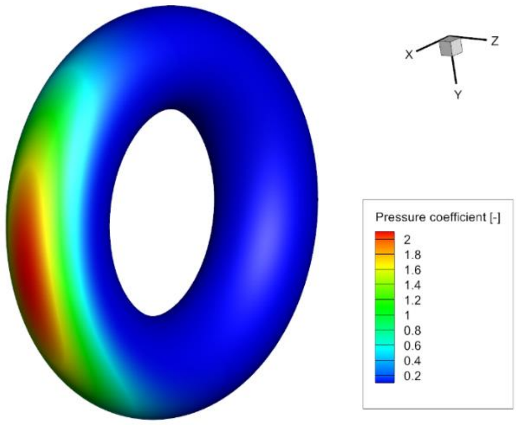

Figure 19 Pressure distribution showing the panels exposed to the flow

6.2 Convective heat flux

The already available panel-based data structure was used to calculate the heat flux on the exterior surface of the vehicle. As in the case of aerodynamic properties, a distinction will be made between the methods for calculating the heat flux according to the flight regimes, namely free molecular, rarefied transitional and continuous. Thus, in the free molecular regime the heat flux was calculated using the molecule-surface interaction theory developed by Schaaf and Talbot in [17]. In the rarefied transitional regime, bridging functions similar to those for the calculation of aerodynamic properties were used ([22], [23]). In the case of the continuous regime, the heat flux was calculated based on correlations with the Fay-Riddell theory for the heat flux at the stagnation point ([23]). The heat flux distribution over the surface of the analyzed vehicle was determined using sphere and cylinder correlations ([24], [25]). More details on the methods are presented in the complete thesis.

6.3 Validation of the computational models

As reference results for the validation of the implemented aerodynamic and aerothermodynamic models, results available in the literature for the Orion capsule were used (Figure 20). The activity presented in [26] is an effort to evaluate the aerodynamic properties of the Orion capsule for several flight regimes, from free molecular hypersonic regime to continuous hypersonic regime, with Knudsen numbers ranging from 111 to 0.0003, and altitudes between 75 and 250 km. For this purpose, the authors of the above-mentioned paper used several well-known computational tools such as the LAURA CFD code developed by NASA and two Monte Carlo codes (Direct Simulation Monte Carlo or DSMC), DS3V (Version 2.4.01) and DAC (DAC97).

For a comparative study, the aerodynamic properties of the Orion capsule were also evaluated using the panel methods described in this chapter. In this regard, a computational grid of triangular elements was generated on the surface of the Orion capsule using the CATIA commercial software, as shown in Figure 21.

Figure 22 and Figure 23 show a comparison between the static aerodynamic characteristics calculated using the implemented methods and those provided by the CFD and DSMC methods in the reference paper. We note that the results provided by the panel models are in good agreement with the CFD and DSMC methods, denoting their good ability to estimate the aerodynamic characteristics for all flight regimes.

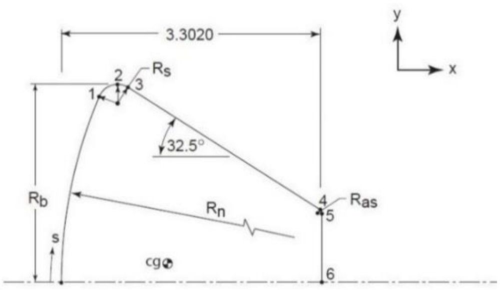

Location	x	y	s
1	0.4812	2.3615	2.4264
2	0.7126	2.5146	2.7203
3	0.8477	2.4752	2.8630
4	3.2785	0.9266	5.7451
5	3.3020	0.8838	5.7961
6	3.3020	0.0000	6.6799
cg	1.3333	0.2414	-

D_b = 5.0292
R_b = 2.5146
R_n = 6.0350
R_s = 0.2515
R_{as} = 0.0508

Dimensions in m

Figure 20 The Orion capsule – geometric properties

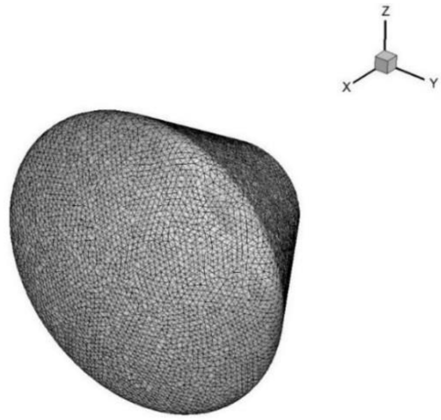

Figure 21 Triangular grid on the Orion capsule

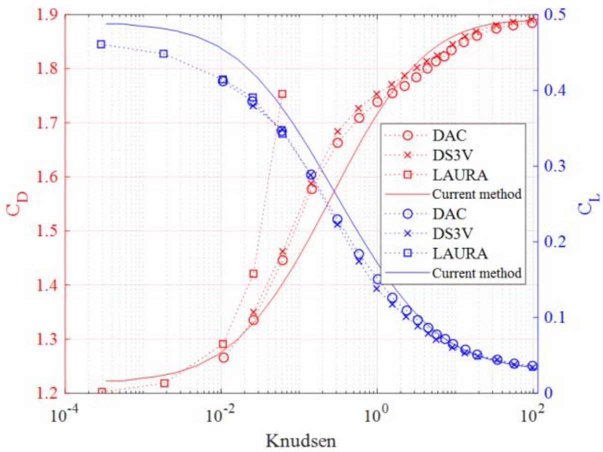

Figure 22 Lift and drag coefficients of the Orion capsule, $V_\infty = 7.6\ km/s, \alpha = 26\ deg$

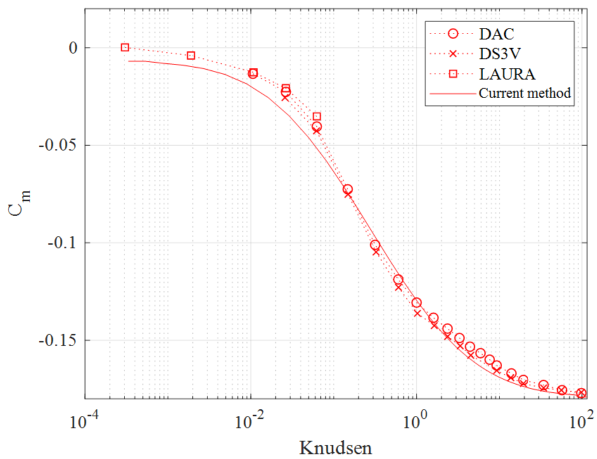

Figure 23 Moment coefficient of the Orion capsule $V_\infty = 7.6\ km/s, \alpha = 26\ deg$

The reference results for the validation of aerothermodynamic models are provided by the paper [27]. Here, distributions of the heat transfer coefficient for the Orion capsule were calculated using two DSMC codes, at altitudes of 95 and 105 km and an angle of attack of 0 degrees. The distribution of the heat transfer coefficient was also calculated using the panel methods presented in this chapter of the thesis. It can be seen in Figure 24 and Figure 25 that the performance of simple engineering methods is acceptable considering their degree of fidelity, especially since differences of up to 25% can be observed even between methods with a high degree of fidelity as DSMC.

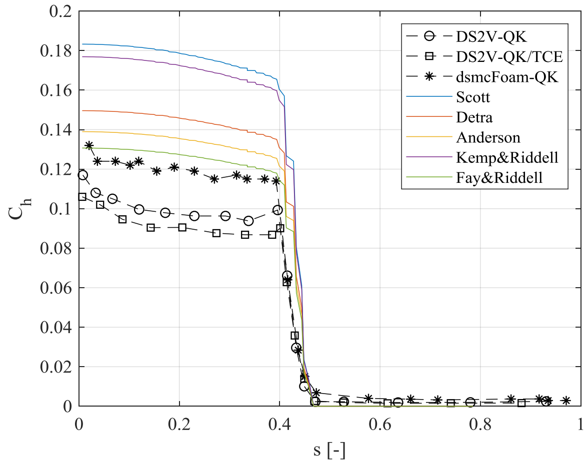

Figure 24 Heat transfer coefficient at 95 km altitude

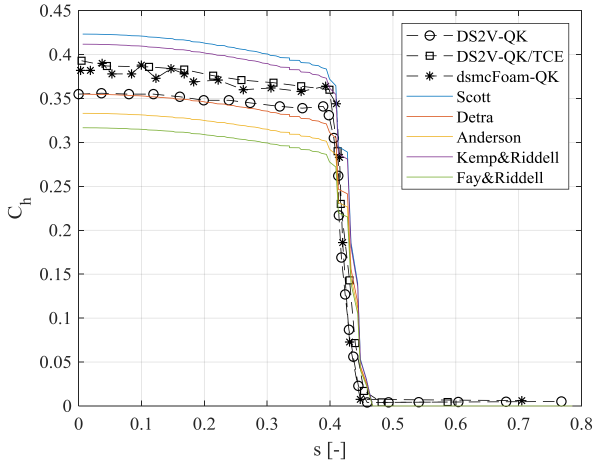

Figure 25 Heat transfer coefficient at 105 km altitude

7 Models of thermal destruction of aerospace vehicles re-entering the atmosphere

7.1 Ablation model for debris re-entering the atmosphere

Fragmentation of a vehicle upon atmospheric re-entry is a complex process that requires the identification and modeling of various phenomena specific to it. For this reason, the calculation algorithm must be able to predict the different ways in which the material of the structure degrades under the influence of thermal and / or mechanical loads. A first step in this regard is a model of erosion (or ablation) of materials under the influence of thermal loads and shear stresses due to air flow, suitable for metallic materials. Such a model was also implemented in this thesis, using the polyhedral data structure generated for the thermal analysis of the vehicle (according to Section 5). The model is based on two main hypotheses:

- The material of the analyzed structure does not degrade in any other way until the melting temperature is reached.
- When parts of the analyzed structure reach melting temperature, the molten material is removed by the air stream.

The implemented erosion model was integrated together with the other calculation models presented throughout the thesis in a complex program capable of simulating the destructive re-entry of a metal object. The logical diagram of the program is shown in Figure 26.

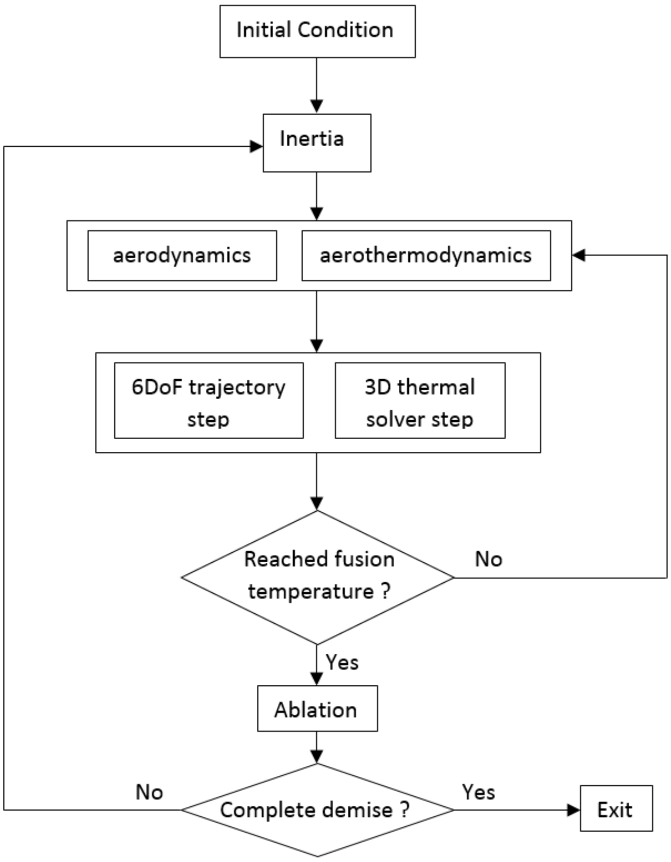

Figure 26 Burn up of a metallic object during reentry – logical scheme

7.2 Ablation model validation

In [28] the authors present experimental results obtained at the von Karman Institute using the Plasmatron experimental facility. In order to validate the ablation model described in this chapter, two experiments performed on a hemispherical sample made of AlSi10Mg (Figure 27), with a thermal stagnation heat setting of 4 MW / m2, were selected. For a comparative study, a computational model of the experimental sample was created, consisting of 1950 hexahedral elements and illustrated in Figure 28.

Figure 27 Experimental model, AlSi10Mg

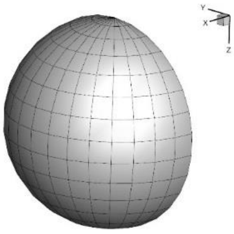

Figure 28 Computational grid

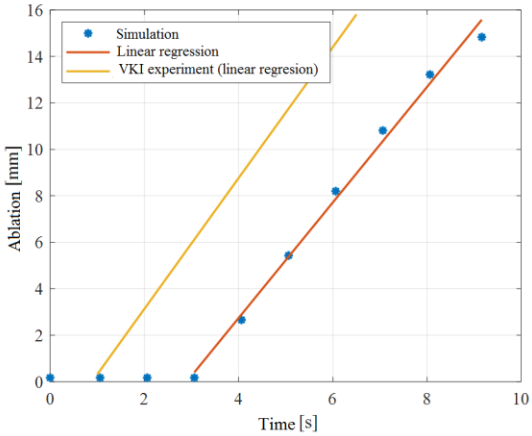

Figure 29 Ablation rate for Al-Si-2bis

Figure 30 shows a comparison between the evolution of the computational model and the experimental sample in the case of the Al-Si-2bis experiment. Here it can be seen that the complete melting time of the sample is about 5 seconds, both in simulation and in experiment. At the same time, the predicted ablation rate of the simulation is consistent with that obtained in the experiment (Figure 29).

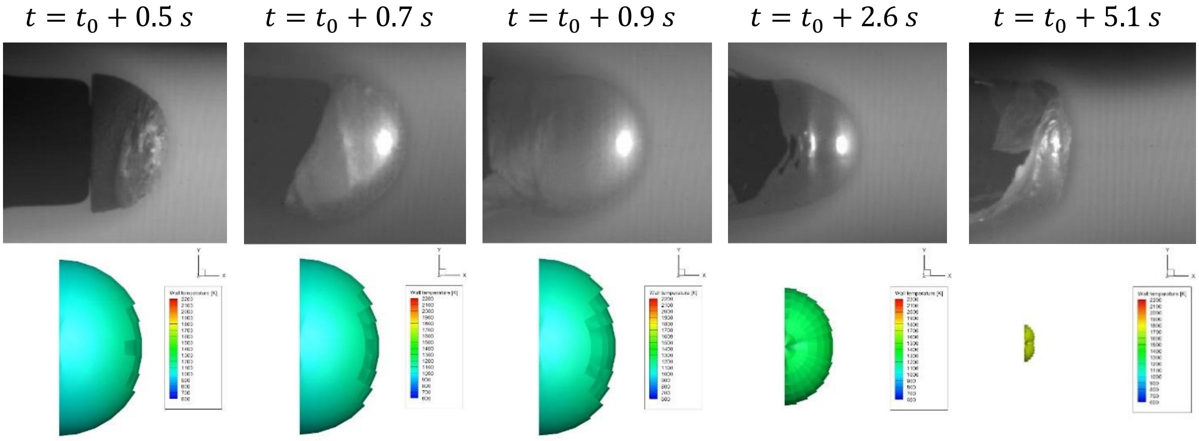

Figure 30 Melting of the AlSi10Mg model – simulation vs. experiment

7.3 Simulation of the destructive re-entry of a metallic object

This paragraph exemplifies the atmospheric destructive re-entry of a metal object, according to the calculation algorithm presented in paragraph 7.1. The re-entry of a cylindrical aluminum object with a mass of 1.52 kg, from an initial altitude of 200 km and an initial speed of 8000 m / s was simulated. Figure 31 shows the evolution of object’s geometry during reentry. It can be seen that, once the melting temperature is reached, the object burns completely in just a few seconds. More details on simulation data and interpretation of results are provided in the complete thesis.

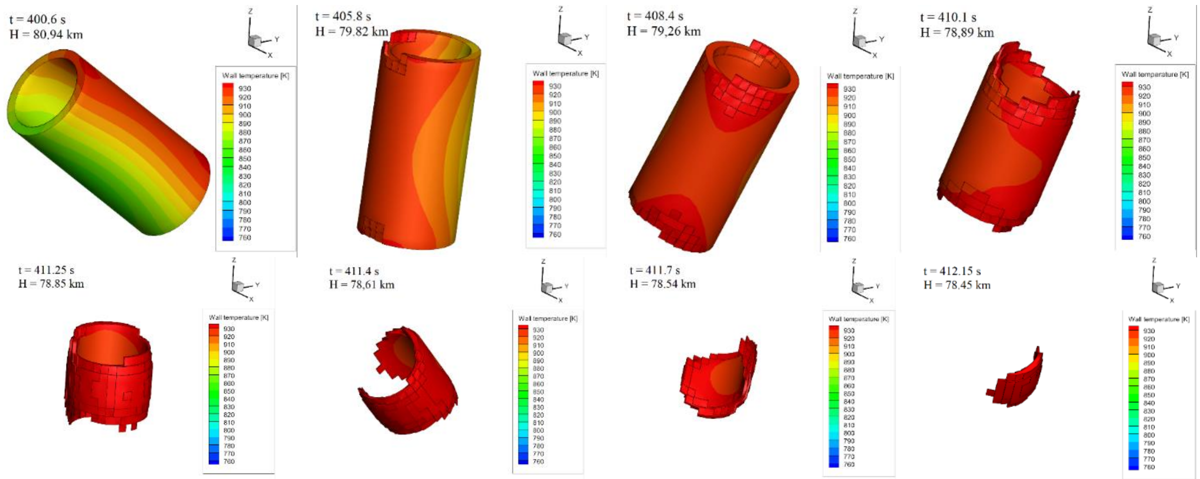

Figure 31 Evolution of the object geometry

7.4 Fragmentation model of complex structures re-entering the atmosphere

A first step in modeling the fragmentation of a vehicle when re-entering the atmosphere is a model of erosion (or ablation) of materials under the influence of thermal loads and shear stresses due to the air flow, suitable for metallic materials. Such an ablation model has been presented in paragraph 7.1 of this thesis. However, the implemented algorithm cannot predict the situations in which the grid that models the analyzed object is no longer connected, which would mean a break up. For this reason, the ablation algorithm has been augmented with a *Depth-First Search* (DFS) algorithm, capable of verifying connections in a computational grid. Figure 33 shows a generic grid with the associated connectivity tree, in which the DFS algorithm is illustrated with blue arrows.

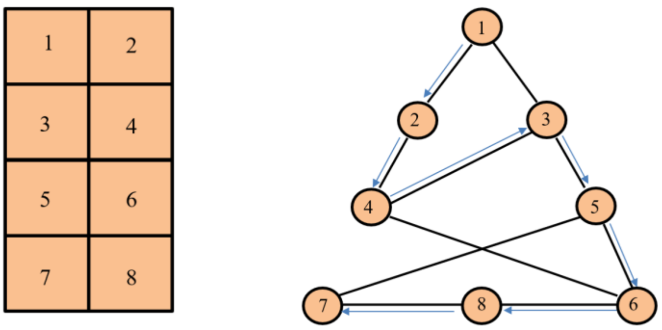

Figure 33 Example of computational grid and its connectivity tree

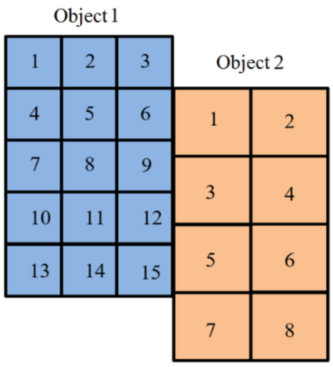

Figure 32 Example of two objects in contact

Fragmentation of the vehicle structure may also occur for other reasons such as the breaking of the mechanical connections holding the objects that make up the structure. In addition, thermal energy can be transferred between neighboring objects in contact. In this respect, assembly interfaces have been defined between the objects of the structure, which can be *mechanical connections*, *thermal connections* or *thermal and mechanical connections*. Following the example of the two connected objects in Figure 32, an assembly interface is materialized at the computational level by the set of cells and interfaces in the immediate vicinity. By means of all the mechanical connections defined between the objects of the structure, a connectivity tree can be defined between them as in Figure 33. When one or more mechanical connections are broken, the connectivity tree between the objects of the structure is checked with the same DFS algorithm above. Thus, the three fragmentation scenarios illustrated in Figure 34 can be distinguished.

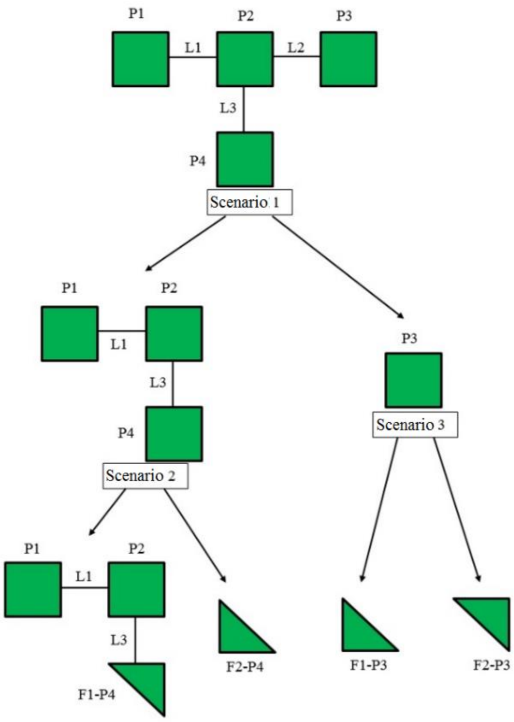

Figure 34 Fragmentation scenarios

7.5 Overview of the practical implementation of the computational models

This paragraph provides details on the practical implementation of all the calculation models presented during the thesis in the MATLAB program. Aspects such as the data structure used and the effective interconnection of the various calculation modules are discussed. All these details can be found in the complete thesis.

7.6 Simulation of the destructive re-entry of a typical rocket stage

The fragmentation algorithm proposed in the previous chapter was tested on a typical launcher stage structure, shown in Figure 35. The structure consists of a total of 67 primitives, of which we can note three tanks, one for oxygen, one for fuel and a one for gas (for RCS), and a payload adapter. In addition, the outer shell of the vehicle consists of a series of transverse and longitudinal elements, to which are added thin sheet metal elements. All the elements that make up the structure are made of 7075 aluminum alloy, except for the three tanks which are made of a titanium alloy TiAl6V4, totaling a mass of about 1200 kg. To simulate the destructive re-entry of the launcher stage, a trajectory starting from 200 km altitude, with an initial speed of 7940 m / s was considered.

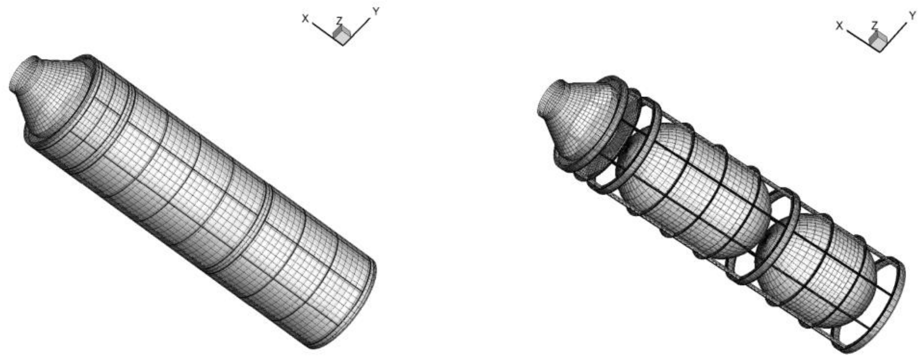

Figure 35 Computational model of the vehicle

A brief summary of the results is presented in Table 4. Here, it can be seen that a total of 475 fragments resulted during re-entry, of which 450 burned completely. As expected, all the fragments that burn during re-entry are made of 7075 aluminum alloy. On the other hand, a total of 25 fragments survive re-entry, of which we can note the three tanks, which arrive unaltered at the point of impact. The latter fact is consistent with observations on real trajectories ([29]) but also with predictions of simulation environments such as the one used in this thesis ([30]). Some of the major fragments resulting from re-entry are illustrated in Figure 38. The state of the vehicle structure up to the time of these important fragmentations is illustrated in Figure 37. Figure 36 shows the trajectories of all resulting fragments, in which fragmentation events are indicated by red dots. We see here that the fragments surviving the re-entry determine an impact footprint of about 400 km in length.

Table 4 Results summary

Initial mass [kg]		Material	Number of fragments	Total number of fragments	Mass [kg]
1198.66	Burned fragments	AA7075	450	450	409.13
	Surviving fragments	Oxygen tank – TiAl6V4, 275 kg	1	25	789.53
		Fuel tank – TiAl6V4, 206 kg	1		
		Gas tank – TiAl6V4, 75 kg	1		
		Other fragments - AA7075	22		

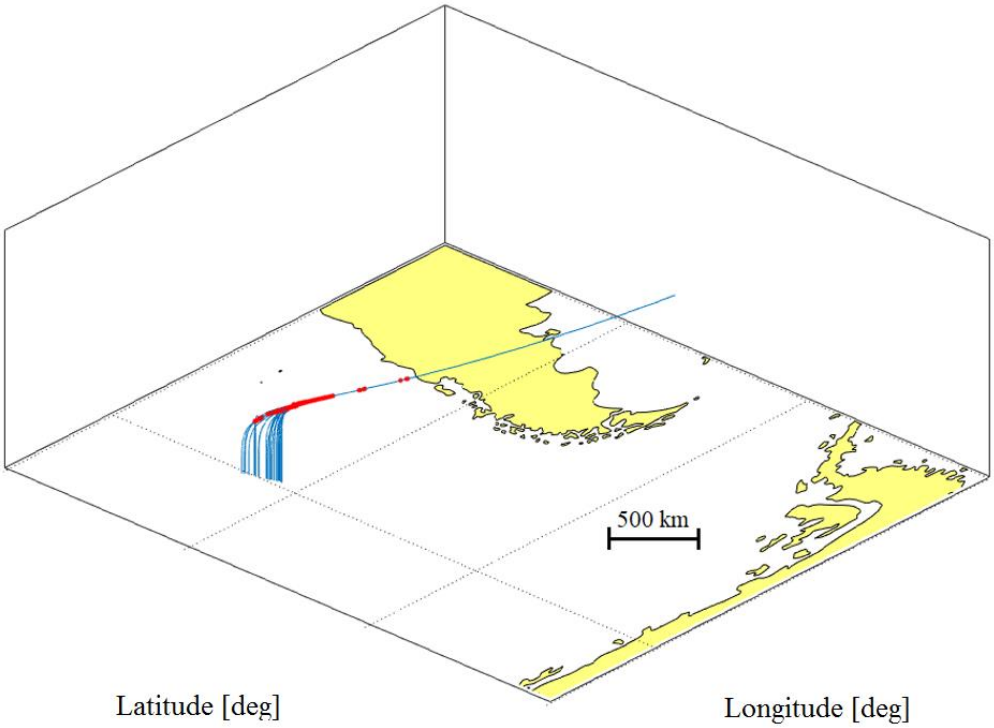

Figure 36 Trajectories of the vehicle and fragments

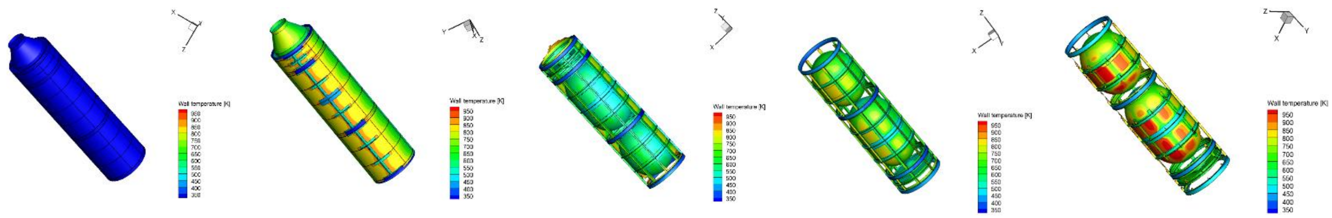

Figure 37 The state of the structure during reentry

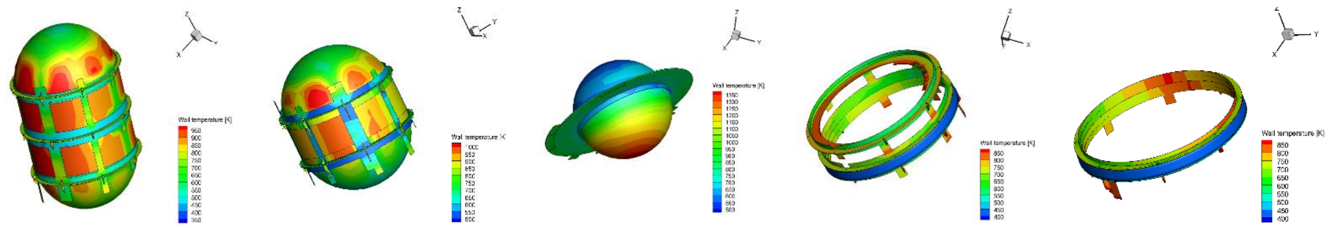

Figure 38 Fragments resulted during reentry

8 Effect of uncertainties

8.1 Introduction

Since the atmospheric destructive re-entry presents very complex phenomena whose understanding requires close intercommunication of several branches of engineering, the use of accurate mathematical models in computational codes capable of simulating such an event is often impossible for practical reasons such as required computational time and resources. For this reason, low-fidelity mathematical models are preferred over high-fidelity ones. These methods of low fidelity bring with them a certain degree of uncertainty which implicitly determines a degree of uncertainty of the results of a simulation. The presence of these uncertainties means that the true result of a simulation is not a singular one but rather a *population* in a statistical sense (infinite size), characterized by a certain set of statistical properties, such as *mean value* or *standard deviation*. To exemplify the determination of the statistical properties of such a population, a Monte Carlo statistical analysis was employed.

8.2 Theoretical aspects regarding the number of iterations and accuracy of a Monte Carlo simulation

In order to determine the number of Monte Carlo iterations needed to accurately capture the statistical properties of the populations of interest, a methodology based on the Central Limit Theorem (TLC), proposed in [31], is adopted. The methodology involves successively extracting samples of progressively larger size from the population of interest until a convergence of the number of iterations required to obtain a desired accuracy is observed. More details are presented in the complete thesis.

8.3 Monte Carlo analysis of a destructive atmospheric re-entry. Example case

A Monte Carlo analysis was exemplified in the case of the destructive re-entry of a generic cylindrical fragment (Figure 39), from an initial altitude of 200 km and an initial speed of 7940 m / s. The fragment consists of two metal objects, an outer shell made of aluminum alloy type aa7075 and a core made of steel type a316. Illustratively, the objective of the Monte Carlo analysis was to determine the statistical properties that describe the coordinates of the point of impact of the object, namely the latitude and longitude of the impact. The analysis was divided into three stages. In the first phase, the nominal trajectory of the object was analyzed in six degrees of freedom up to a value of the Mach number of 5 (limit of the hypersonic regime), followed by an analysis in three degrees of freedom until the impact (see also the explanations in 7.5). In the second stage, the sensitivity of the impact point to the uncertainties associated with each of the uncertain parameters was analyzed. As in the case of the nominal trajectory, the analysis was made in six degrees of freedom, successively and individually perturbing one of the parameters or uncertain quantities at their minimum and maximum values (limits of the uncertainty range). In the third stage, the actual Monte Carlo analysis was performed. This time, the whole trajectory was analyzed with only three degrees of freedom with a fixed attitude, varying the initial attitude each time a simulation with perturbed parameters was performed.

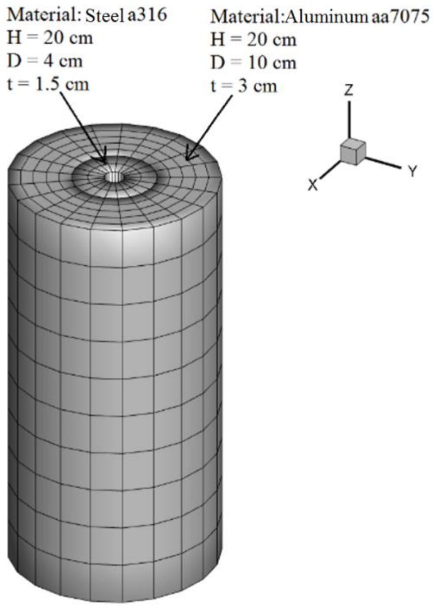

Material properties	Aluminum	Steel
Density:	2810	8030 kg/m^3
Melting temperature:	870	1650 K
Thermal conductivity:	130	16.3 W/mK
Specific heat:	910	510 J/kgK
Initial temperature:	300	300 K

Inertial properties (total)	
Mass:	5.516 (3.65 / 1.86) kg
Moment of inertia I_{xx}:	0.0212 kgm^2
Moment of inertia I_{yy}:	0.0212 kgm^2
Moment of inertia I_{zz}:	0.0056 kgm^2

Figure 39 Inertial and material properties

Altitude and downrange during nominal reentry are shown in Figure 40. Sensitivity of the point of impact to the various categories of uncertain parameters is illustrated in Figure 41. Figure 42 shows that the entire aluminum outer shell melts during the nominal reentry of the object.

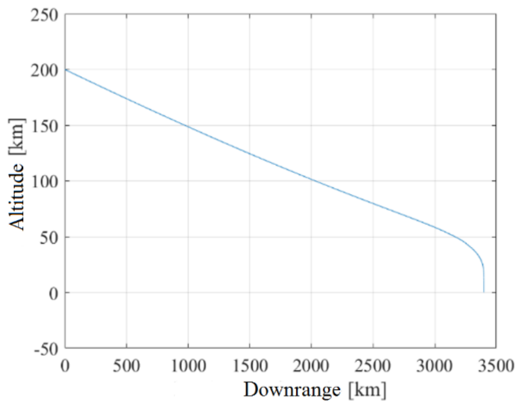

Figure 40 Altitude and downrange of the object (Nominal, 6DoF)

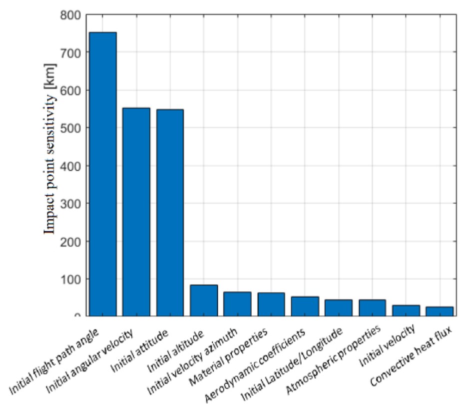

Figure 41 Sensitivity of the impact point to uncertainties

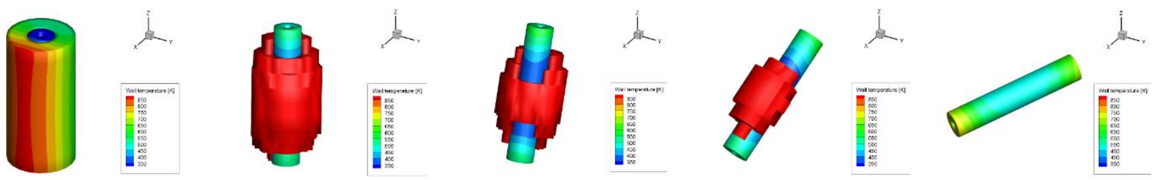

Figure 42 Evolution of the object geometry (Nominal, 6DoF)

In order to determine the statistical properties that describe the coordinates of the impact point of the object, a number of 5000 perturbed trajectories were simulated. The coordinates of the impact point, altitude and downrange of the object for all 5000 trajectories are shown in Figure

43 and Figure 44. Here it can be seen a very high degree of scattering of the coordinates of the impact point, with downrange ranging from 2600 to 7800 km. This result is mainly due to the uncertainties considered on the initial flight path angle and the initial attitude of the object, as shown in Figure 41. More details on the simulations and interpretation of the results can be found in the complete thesis.

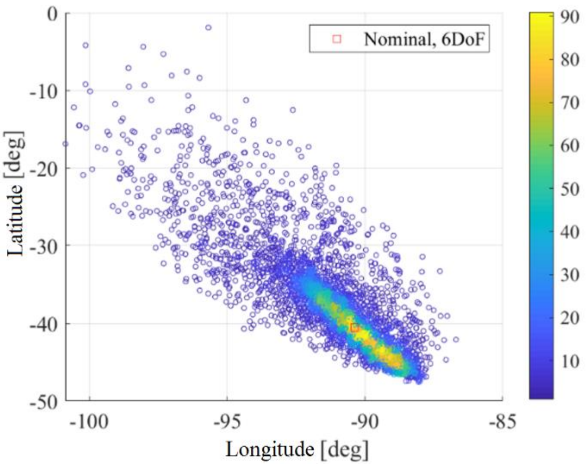

Figure 43 Coordinates of the impact point

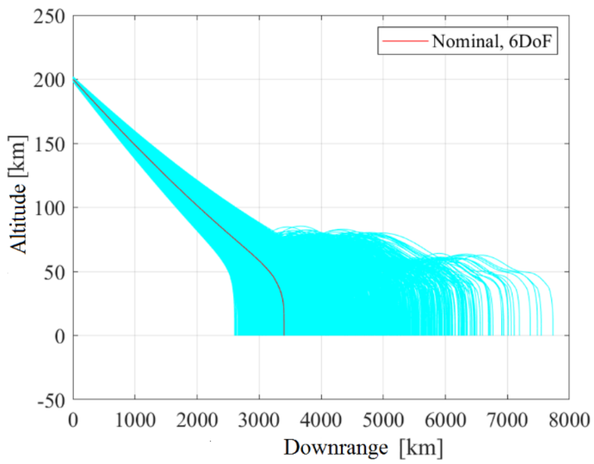

Figure 44 Altitude and downrange of the object

9 Final chapter

9.1 Thesis contributions

Given the growing interest in the development of computational tools for simulating atmospheric destructive re-entry, this thesis aimed to identify a collection of mathematical models suitable for inclusion in such a multidisciplinary computing environment. A first merit of this thesis is to identify and present in detail models associated with several branches of engineering such as trajectory analysis, aerodynamics, aerothermodynamics and heat transfer and to unify them at a practical level in a complex calculation code. The merit is even greater as the calculation code is the first of its kind developed in Romania's scientific community, and as Romania's interest in European projects focused on space missions is growing. The calculation code was implemented in the MATLAB programming environment and includes several modules, which can also be used individually. So, we can list:

1. A trajectory simulator capable of simulating the motion of spacecraft in both three and six degrees of freedom. The code encompasses several sets of equations of motion determined based on Newtonian principles and advanced planetary models, gravity and atmosphere. (details in section 4).
2. A heat transfer simulator capable of numerically solving the heat equation on three-dimensional unstructured grids. The code implements a finite volume method specific to unstructured grids that uses an advanced implicit time integration algorithm (details in section 5).
3. A module for generating and preprocessing computational grids. This module is able to automatically generate unstructured three-dimensional grids for a series of objects with simple geometry, based on input parameters. At the same time, data structures specific to

unstructured grids such as connectivity, geometric properties, boundary information, are computed automatically. The module also offers the possibility to assemble several grids in order to generate a complex structure.

4. A module for calculating inertial properties. The calculation module is able to estimate very efficiently and with very high accuracy the inertial properties of a structure no matter how complex, based on a grid or sets of grids that define the given structure.
5. A module for calculating aerodynamic characteristics and convective heat flux. This code has the ability to estimate the aerodynamic characteristics and distribution of convective heat flux by using methods based on the local inclination of the object surface relative to the direction of the air flow. The code also includes a parallel shading algorithm that makes it possible to determine those panels (surface elements of the analyzed vehicle) that are exposed directly to the air flow.

Although their degree of impact remains to be demonstrated, this thesis includes several original ideas:

1. A fragmentation algorithm for complex structures during atmospheric re-entry. This thesis proposes in paragraph 7.4 an original algorithm for fragmentation of spacecraft structures upon atmospheric re-entry. The algorithm is based on the definition of mechanical interfaces (which can mean effective physical assembly links) between objects that make up the structure of a vehicle, materialized by sets of elements belonging to the grids of objects in contact or in the immediate vicinity. Based on them, a connectivity tree of the whole vehicle is created whose connections are checked at each step of the simulation by means of a *Depth-First Search* (or *DFS*) algorithm. A mechanical connection between two objects is considered broken when all the elements that define the interface are removed following the melting of the material under the influence of thermal loads. Thus, the proposed algorithm models the fragmentation of structures by predominantly thermal considerations.
2. Refining an existing shading algorithm. Section 6 of this thesis presents a shading algorithm based on an approach already existing in the literature. The proposed new algorithm is intended to improve computation time by minimizing the number of panel-by-panel checks, by vectorizing computation operations, and by execution on multiple processors.
3. In section 6 of this thesis, a methodology for estimating the drag coefficient of fragments with random geometry in the subsonic, transonic and supersonic regimes is presented. The method is based on an existing approach in which a drag profile as a function of Mach is defined based on a known anchor point and known data for objects with regular geometry. The novelty of the presented methodology is to define the anchor point as an average value of the drag coefficient derived from the analysis in six degrees of freedom of the object in the hypersonic regime. Thus, the drag profile is calibrated based on the results provided by the panel-based methods in the hypersonic regime, methods that have a good accuracy in this flight regime. At the same time, the proposed methodology is one that facilitates statistical analyzes such as Monte Carlo, in the sense that the points that define the drag profile can be directly perturbed.

4. Section 5 of the thesis presents in detail the methodology of numerical solution of the heat equation on unstructured grids. The novelty is that the presented methodology is an adaptation of algorithms that are specific to the computational fluid dynamics (CFD) methods for the case of the heat equation. Therefore, the present thesis proposed the use of the dual time method for the temporal propagation of the numerical solution of the heat equation. The method is based on the idea of solving a steady state problem at every physical time step. Although in the literature, the steady state problem in heat transfer is defined by the Laplace or Poisson equation (without time derivative), this thesis proposed the use of a CFD-specific implicit method, in which the solution is propagated in a fictitious time using an implicit algorithm. The fictitious time propagation algorithm is very efficient because it can use very large CFL numbers and because it uses simple methods to solve the linear system such as Jacobi or Gauss-Seidel, which can be fully vectorized. Adapting these methods to the heat equation case made it possible to derive the expression of the numerical flux Jacobian of the heat equation and to propose a methodology for numerically implementing the implicit boundary conditions. The latter can be easily extended to numerical solution methods for fluid dynamics. It is important to note that the entire methodology used for the numerical solution of the heat equation is one born out of pure practicality and the present thesis did not present detailed numerical analyzes in this regard. The validity and effectiveness of the method remain to be demonstrated in further research.

9.2 Conclusions and possibilities for further development

This thesis addressed the topic of simulating the destructive re-entry of space vehicles and debris. The overall objective was to identify and implement a series of computational models associated with areas such as trajectory analysis, aerodynamics, aerothermodynamics, heat transfer, in order to pave the way for the creation of a multidisciplinary tool capable of simulating the destructive re-entry of vehicles and space debris and assess the risk involved. For this reason, the thesis was divided into chapters representing specific studies of certain disciplines that participate in the process of developing a multidisciplinary computational tool.

Considering the complexity of the problem that was the subject of this thesis, we can easily identify aspects that need improvement or have not yet been covered throughout the thesis. Therefore, depending on the discipline in which further developments can be made, we can discuss:

- *Structural analysis* - In order to increase the fidelity of the computational tool it is desirable that during further research to consider the implementation of a calculation module capable of determining the internal mechanical stresses of the structure of the analyzed vehicle. Based on it, additional fragmentation models can be built on both thermal and mechanical basis. A possible approach would be to define mechanical interfaces between the objects that make up the structure (similar to the thermal interfaces defined in paragraph 7.4), which may be subjected to a stress analysis under the effect of relative forces between objects, due to both pressure distribution and inertial loads associated with strong decelerations in the atmosphere. Of course, the implementation of higher fidelity models such as those based on finite element theory can also be considered. At the same time, different forms of failure of the structure of the analyzed vehicle can be considered, depending on the type of materials that make it up.

- *Aerodynamics / Aerothermodynamics* - As most specific computational tools do, aerodynamic characteristics and convective heat flux were estimated throughout this work using low fidelity models based on simple engineering correlations. Based on future or existing experimental or numerical results, new empirical calculation models may be proposed or a calibration of existing models may be attempted. One of the key tools in determining the aerodynamic characteristics is represented by the so-called shading algorithm, discussed and implemented in this work. The use of such an algorithm has the disadvantage that it has a very high computational effort (over 50-60% of the total effort), which can open the subject of attempts to improve such algorithms or to propose new ones.
- *Thermal analysis* - The studies carried out throughout this work are only suitable for homogeneous and isotropic materials such as metals. Given the growing interest in the use of composite materials in spacecraft structures, an open topic remains to identify and implement appropriate heat transfer simulation methods for these types of materials.
- *Validation* - To increase the confidence level of the implemented computational models, additional validation cases can be identified and provided. Future or existing experimental and numerical results could be considered for further validation of aerodynamic and aerothermodynamic models. At the same time, a validation of the thermal solver can be done with the help of an already existing and validated solver. In addition to the individual validation of the various computational modules involved in the analysis of a destructive re-entry, as was done in this thesis, a global validation of the entire computational suite is required in order to consider how the different methods are interconnected. The latter method of validation is meant to quantify the degree of realism that fragmentation models like the one proposed in this thesis present. Such a validation of a computational suite for destructive re-entry is difficult as there are not enough observations of real atmospheric re-entries, and assembling high-fidelity methods for validation is also a difficult task.
- *Uncertainties* - Due to the incomplete understanding of the phenomenon that govern atmospheric re-entry or the inability to use high fidelity models, most computational tools are based on simple engineering methods that have a high degree of uncertainty. In this respect, it is necessary to carefully quantify these uncertainties in order to be used in statistical analyzes such as Monte Carlo. At the same time, in the perspective of performing Monte Carlo analyzes on more complex models, it is also of interest to optimize the numerical implementation of all computational algorithms involved in the simulation of a destructive re-entry.

9.3 List of publications

During the elaboration of this thesis, a number of 9 scientific articles were published, one of which as the main author.

1. **T. P. Afilipoae**, A. M. Neculăescu, A. I. Onel, M. V. Pricop, A. Marin, A. G. Perşinaru, A. M. Cişmilianu, I. C. Oncescu, A. Toader, A. Sirbi, S. Bennani, T. V. Chelaru, "Launch Vehicle - MDO in the development of a Microlauncher," *Transportation Research Procedia*, vol. 29, pp. 1-11, 2018. ISSN: 2352-1465. - **ISI, WOS: 000454701600001**
2. A. M. Neculăescu, **T. P. Afilipoae**, A. I. Onel, M. V. Pricop, I. Stroe, "Trajectory Optimization For Small Launchers Using A Genetic Algorithm Approach," 12th International Conference on Mathematical Problems in Engineering, Aerospace and Sciences (ICNPAA), Yerevan, Armenia, 3 - 6 July 2018, *AIP Conference Proceedings,* vol. 2046, 2018. ISBN: 978-0-7354-1772-4, - **ISI, WOS: 000468353100063**
3. T. V. Chelaru, A. I. Onel, **T. P. Afilipoae**, A. M. Neculăescu, "Mathematical Model for Microlauncher performances evaluation," *UPB Scientific Bulletin, Series D: Mechanical Engineering,* vol. 79, nr. 4, pp. 49-66, 2017. ISSN: 1454–2358. - **SCOPUS**
4. T. V. Chelaru, V. Pană, A. I. Onel, **T. P. Afilipoae**, A. F. Cojocaru, I. C. Vasile, "Flexible model for Micro-Launcher Dynamics," Proceedings of 9th International Conference on Innovation in Aviation & Space-EASN, 3-6 September 2019, Athens, Greece, *MATEC Web of Conferences,* vol. 304, 2019. ISSN: 2261-236X. - **BDI: DOAJ**
5. T. V. Chelaru, V. Pană, A. I. Onel, **T. P. Afilipoae**, A. F. Cojocaru, I. C. Vasile, "Wind Influence on Micro-Launcher Dynamics Model," Proceedings of 9th International Conference on Innovation in Aviation & Space-EASN, 3-6 September 2019, Athens, Greece, *MATEC Web of Conferences,* vol. 304, 2019. ISSN: 2261-236X. - **BDI: DOAJ**
6. A. I. Onel, **T. P. Afilipoae**, A. M. Neculăescu, M. V. Pricop, "MDO approach for a two-stage microlauncher," *INCAS Bulletin,* vol. 10, nr. 3, pp. 127-138, 2018. (P) ISSN: 2066–8201, (E) ISSN: 2247–4528. - **SCOPUS**
7. A. I. Onel, A. Stăvărescu, M. G. Cojocaru, M. V. Pricop, M. L. Niculescu, A. M. Neculăescu, **T. P. Afilipoae**, "Computation of the Hypersonic Heat Flux with Application to Small Launchers," 12th International Conference on Mathematical Problems in Engineering, Aerospace and Sciences (ICNPAA), Yerevan, Armenia, 3 - 6 July 2018, *AIP Conference Proceedings,* vol. 2046, 2018. ISBN: 978-0-7354-1772-4, - **ISI, WOS: 000468353100067**
8. A. I. Onel, **T. P. Afilipoae**, A. M. Neculăescu, M. V. Pricop, "Drag coefficient modelling in the context of small launcher optimisation," *INCAS Bulletin,* vol. 10, nr. 4, pp. 103-116, 2018. (P) ISSN: 2066–8201, (E) ISSN: 2247–4528. - **SCOPUS**
9. A. I. Onel, O. I. Popescu, A. M. Neculăescu, **T. P. Afilipoae**, T. V. Chelaru, "Liquid rocket engine performance assessment in the context of small launcher optimisation," *INCAS Bulletin,* vol. 11, nr. 3, pp. 135-145, 2019. (P) ISSN 2066–8201, (E) ISSN 2247–4528. – **SCOPUS**

Bibliography

[1] C. D. Persis, „A risk assessment tool for highly energetic break-up events during the atmospheric re-entry,” The University of Dublin, 2017.

[2] T. M. Owens, „Aero-thermal Demise of Reentry Debris - A computational model,” Florida Institute of Technology, 2013.

[3] J. C. Stroup, „Assessment of risk for human casualty from atmospheric reentry,” Naval Postgraduate School, Monterey, California, 2016.

[4] M. McWinnie, „Health monitoring of re-entry vehicles,” Cranfield University, 2011.

[5] W. Ziniu, H. Ruifeng, Q. Xi, W. Xiang și W. Zhe, „Space Debris Reentry Analysis Methods and Tools,” *Chinese Journal of Aeronautics,* vol. 24, pp. 387-395, 2011.

[6] P. Omaly și M. Spel, „DEBRISK, a tool for re-entry risk analysis,” în *IAASS Conference*, Versailles, 2011.

[7] V. Braun și J. G. e. al., „DRAMA 2.0 - ESA’S SPACE DEBRIS RISK ASSESSMENT AND MITIGATION ANALYSIS TOOL SUITE,” 2013.

[8] J. Merrifield și J. B. e. al., „AEROTHERMAL HEATING METHODOLOGY IN THE SPACECRAFT AEROTHERMAL MODEL (SAM),” 2014.

[9] G. Koppenwallner, B. Fritsche, T. Lips și H. Klinkrad, „SCARAB - A Multi-Discilplinary Code for Destruction Analysis of Space-Craft During Re-entry,” în *Fifth European Symposium on Aerothermodynamics for Space vehicles*, Cologne, 2005.

[10] A. Salama, L. Ling și A. McRonald, „A Genesis Breakup and Burnup Analysis in Off-Nominal Earth Return and Atmospheric Entry,” în *Global Aerospace,* Pasadena, California.

[11] J. Annaloro, S. Galera, P. Kärräng, G. Prigent, T. Lips și P. Omaly, „Comparison between two spacecraft-oriented tools: PAMPERO & SCARAB,” *The Journal of Space Safety Engineering,* vol. 4, pp. 15-21, 2017.

[12] J. Annaloro, P. Omaly, V. Rivola și M. Spel, „Elaboration of anew spacecraft-oriented tool: PAMPERO,” în *8th European Symposium on Aerothermodynamics for Space Vehicles,* Lisbonne, 2015.

[13] D. Eberly, „Polyhedral Mass Properties (Revisited),” Geometric Tools, 2009.

[14] ASTOSSolutions, „ASTOS 8 User manual," ASTOS Solutions, 2015.

[15] K. H. Y. I. Nobuaki IShii, „Attitude motion and aerodynamic characteristics of MUSES-C reentry capsule," The Institute of Space and Astronautical Science, 2003.

[16] A. Jameson, „Time Dependent Calculations Using Multigrid, with Applications to Unsteady Flows Past Airfoils and Wings," *AIAA Journal,* 1991.

[17] S. A. Schaaf și L. Talbot, „Handbook of supersonic aerodynamics," University of California, 1959.

[18] P. Gallais, Atmospheric Re-Entry Vehicle Mechanics, Springer, 2007.

[19] A. Sreekanth, Aerodynamic Predictive Methods And Their Validation In Hypersonic Flows, New Delhi: Defence Research & Development Organisation, 2003.

[20] F. Mccleskey, „Drag coefficient for irregular fragments," Naval Surface Warfare Center, 1988.

[21] D. Mostaza-Prieto, „Characterisation and Applications of Aerodynamic Torques on Satellites," School of Mechanical, Aerospace and Civil Engineering, 2017.

[22] H. Legge, „Hypersonic approximations for heat transfer and shear stress applied to continuum and rarefied plume impingement," 1987.

[23] A. Viviani și G. Pezzella, Aerodynamic and Aerothermodynamic Analysis of Space Mision Vehicles, Springer, 2015.

[24] J. A. Merrifield, „Aerothermal Heating Methodology in the Spacecraft Aerothermal Model," 2014.

[25] G. Koppenwallner, „SCARAB - A Multi-Disciplinary Code for Destruction Analysis of Space-Craft During Re-entry".

[26] J. N. Moss, K. A. Boyle și F. A. Greene, „Orion Aerodynamics for Hypersonic Free Molecular to Continuum Conditions," *14th AIAA/AHI International Space Planes and Hypersonic Systems and Technologies Conference,* 2006.

[27] R. C. Palharini, *Atmospheric Reentry Modelling Using an Open-Source DSMC code,* University of Strathclyde, 2014.

[28] B. Helber, O. Chazot, T. Afilipoae, M.-V. Pricop și J.-P. Preaud, „Metallic Alloy and CFRP Demise Ablation Tests in the VKI Inductively-Coupled Plasmatron," 2019.

[29] W. Ailor, W. Hallman, G. Steckel și M. Weaver, „Analysis of Reentered Debris and Implications for Survivability Modeling,” în *Proceedings of the Fourth European Conference of Space Debris*, Darmstadt, 2005.

[30] R. G. Stern, „Analysis of Mir Reentry Breakup,” Space and Missle Systems Center, Los Angeles, 2003.

[31] W. Oberle, „Monte Carlo Simulations: Number of Iterations and Accuracy,” US Army Research Laboratory, 2015.